Ootes, L., Snyder, D., Davis, W. J., Acosta-Góngora, P., Corriveau, L., Mumin, A., Gleeson, S. A., Samson, I. M., Montreuil, J.-F., Potter, E., Jackson, V. A. (2017): A Paleoproterozoic Andean-type iron oxide copper-gold environment, the Great Bear magmatic zone, Northwest Canada. - *Ore geology reviews*, *81*, Pt.1, pp. 123—139.

DOI: http://doi.org/10.1016/j.oregeorev.2016.09.024

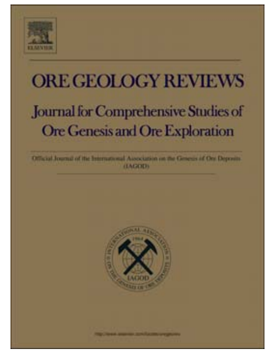

A Paleoproterozoic Andean-type iron oxide copper-gold environment, the Great Bear magmatic zone, Northwest Canada

Luke Ootes, David Snyder, William J. Davis, Pedro Acosta-Góngora, Louise Corriveau, A.Hamid Mumin, Sarah A. Gleeson, Iain M. Samson, Jean-François Montreuil, Eric Potter, Valerie A. Jackson

PII:	S0169-1368(16)30166-4
DOI:	doi:10.1016/j.oregeorev.2016.09.024
Reference:	OREGEO 1948
To appear in:	*Ore Geology Reviews*
Received date:	30 March 2016
Revised date:	15 September 2016
Accepted date:	19 September 2016

Please cite this article as: Ootes, Luke, Snyder, David, Davis, William J., Acosta-Góngora, Pedro, Corriveau, Louise, Mumin, A.Hamid, Gleeson, Sarah A., Samson, Iain M., Montreuil, Jean-François, Potter, Eric, Jackson, Valerie A., A Paleoproterozoic Andean-type iron oxide copper-gold environment, the Great Bear magmatic zone, Northwest Canada, *Ore Geology Reviews* (2016), doi:10.1016/j.oregeorev.2016.09.024

A Paleoproterozoic Andean-type iron oxide copper-gold environment, the Great Bear magmatic zone, Northwest Canada

[1*]Luke Ootes, [2]David Snyder, [2]William J. Davis, [2,3]Pedro Acosta-Góngora, [4]Louise Corriveau, [5]A.Hamid Mumin, [3,6]Sarah A. Gleeson, [7]Iain M. Samson, [8]Jean-François Montreuil, [2]Eric Potter, and [1**]Valerie A. Jackson

1. Northwest Territories Geological Survey, Box 1320, Yellowknife, Northwest Territories, Canada X1A 2L9
2. Geological Survey of Canada, 601 Booth Street, Ottawa, ON, Canada K1A 0E8
3. Department of Earth and Atmospheric Sciences, University of Alberta, Edmonton, Alberta, Canada T6G 2E3
4. Geological Survey of Canada, 490 rue de la Couronne, Québec, QC, G1K9A9
5. Department of Geology, Brandon University, Brandon, Manitoba, R7A 6A9
6. Helmholtz Centre Potsdam, GFZ German Research Centre for Geosciences, Section 3.1: Inorganic and isotope geochemistry, Telegrafenberg B121, 14473 Potsdam, Germany
7. Department of Earth and Environmental Sciences, University of Windsor, Windsor, Ontario, Canada N9B 3P4
8. Red Pine Exploration, 141 Adelaide Street West, suite 520, Toronto , ON, M5H 3L5

Corresponding author:
Luke.ootes@gov.bc.ca

*current address:
British Columbia Geological Survey
Box 9333 Stn Prov Govt
Victoria, BC, V8W 9N3

** 3126 Westridge Pl
Victoria, BC
V9E 1C8

Abstract

Iron oxide copper-gold (IOCG) and associated iron-oxide apatite (IOA) styles of metallic mineralization are recognized throughout the Paleoproterozoic Great Bear magmatic zone of the northwest Canadian Shield. The Great Bear magmatic zone was constructed between ca. 1876 and 1855 Ma on top of the older Hottah terrane, which preserves continental arc magmatism that began around ca. 2.0 to 1.97 Ga and continued between ca. 1.93 and 1.89 Ga. The Great Bear represents the final stages of ca. 150 million years of intermittent and pulsed magmatism related to an evolving continental orogenic belt. The preserved geology supports a dramatic geodynamic change in the subduction zone process at ca. 1875 Ma, a key driving mechanism for magma and metal mobilization, and was rapidly followed by a large-scale introduction of felsic-intermediate plutons. The overall tectonic setting is partially constrained from new and previously published geochemical data that show that the volcanic and plutonic rocks are high-K calc-alkaline to shoshonitic in nature (e.g., high K_2O, Th/Yb, and Ce/P_20_5). They also have suprasubduction-zone geochemical signatures, including primitive mantle normalized positive Th and negative Nb, P, and Ti anomalies. The data support the primary melts were derived from a GLOSS-modified mantle wedge. Three-dimensional rendering of geophysical datasets suggest that two (of four) preserved surfaces within the upper mantle lithosphere, at 70 to 120 km depths, represent frozen, subducted oceanic slabs, and likely were the drivers for the bulk of Hottah and Great Bear arc magmatism. The older slab is northwest-striking and dips 12° to 15° northeast, whereas the younger is deeper and north-striking, dipping 13° east. The geometry of the surfaces are comparable with 4D modeling, where a subduction zone is temporarily shut down due to plateau collision, and then steps oceanward and re-initiates; there is no need for polarity reversal of the subduction system. This new geometry and the related inferences about process should be the focus of future research in the region, but for the time-being it can be stated that these subduction and collisional processes were the first order control on lithospheric evolution, and therefore metallic mineralization. Overall, the Great Bear magmatic zone IOCG and related mineralization is not comparable to other Proterozoic IOCG belts, such as those in Australia. However, the complexity of mineralization styles, the spatial-temporal relationship between IOA and IOCG mineralization, the suprasubduction zone environment, and a major change in tectonic regime are features similar to Andean-type IOCG mineralization, as well as Cordilleran alkali porphyry Cu-

Au deposits. This further establishes the linkages between subduction zone processes and IOCG formation, as well as relationships in the IOCG-porphyry deposit continuum model.

1. INTRODUCTION

The iron oxide copper-gold (IOCG) deposit model was initiated to help explain a series of somewhat disparate hydrothermal iron-oxide rich mineralization types (Hitzman et al., 1992). This has since been updated to be both inclusive and exclusive of a variety of mineralization styles (Williams et al., 2005; Corriveau, 2007; Groves et al. 2010; Chen, 2013). The original IOCG definition of Hitzman et al. (1992), followed by Williams et al. (2005), has been streamlined in some recent classifications that have removed iron-oxide-apatite (IOA) from the IOCG model (Groves et al. 2010; Chen, 2013), while others continue to show a possible relationship between magmatic-hydrothermal IOCG and IOA deposits (e.g., Mumin et al., 2010; Smith et al., 2012; Richards and Mumin, 2013a). Groves et al. (2010) suggest that the only examples where IOA-type and IOCG deposits are related to one another are in Mesozoic and Cenozoic Andean-like convergent margin-settings (ie. the Mesozoic deposits in Chile and Peru; Sillitoe, 2003; Barton et al., 2013; Chen et al., 2013).

The ca. 1875 to 1850 Ma Great Bear magmatic zone has long been considered a Paleoproterozoic example of a convergent margin volcano-plutonic complex. As early as 1973, it was shown to contain predominantly K-rich, calc-alkaline igneous rocks, interpreted to be consistent with a trench-distal subduction origin (Badham, 1973). That work has since been extensively built upon and a continental arc environment, with similarities to many continental volcanic arcs, was further substantiated for Great Bear magmatism (Hildebrand, 1981; Hildebrand et al., 1987; Gandhi et al., 2001). It was hypothesized that Great Bear magmatism was driven by eastward-directed subduction and was built upon the older crust of the Hottah terrane and western Slave craton (Hildebrand, 1981; Hildebrand et al., 1987, 2010a; Ootes et al., 2015). Uranium-lead zircon dating of volcanic and intrusive phases has pinned this magmatism between ca. 1876 and 1855 Ma (Bowring, 1984; Gandhi et al., 2001; Bennett and Rivers, 2006a; Davis et al. 2011; Ootes et al., 2015). The Slave-Northern Cordillera Lithospheric Evolution (SNORCLE) geophysical transect yielded a seismic profile that imaged east-dipping reflections interpreted to be a frozen, subducted oceanic slab under the Great Bear magmatic zone and western Slave craton, and independently validated the subduction-related hypothesis for the evolution of the Great Bear magmatic zone (Cook et al., 1999). This frozen slab was further defined by related datasets utilizing magnetotelluric, teleseismic, and wide-angle refraction data

(Bostock, 1998; Cook and Erdmer, 2005; Clowes et al., 2005; Wu et al., 2005, Oueity and Clowes, 2010).

Iron oxide copper-gold styles of mineralization and IOA ± actinolite mineralization are recognized throughout the Great Bear magmatic zone, where they are spatially and temporally related to one another and extensive magmatism (Badham and Morton, 1976; Hildebrand, 1986; Gandhi, 1994; Goad et al., 2000; Mumin et al., 2007, 2010; Corriveau et al., 2010a, b; Ootes et al., 2010; Potter et al., 2013; Somarin and Mumin, 2014; Acosta-Góngora et al., 2014, 2015a, b, accepted with revisions; Mumin, 2015). We present a large-scale overview of the Great Bear magmatic zone and its geodynamic setting. The IOCG and IOA deposits fit in a tight time-window, and we link the deposits and the associated magmatism with a convergent margin-like subduction origin, albeit during an extensional relapse (Mumin et al., 2014). The results also provide new insights into the geometry and petrologic evolution of the region. This study supports the suggestion that this Paleoproterozoic metallogenic zone is not directly comparable to many other Precambrian IOCG examples (Groves et al., 2010), but rather we show it is comparable to the Andean styles of IOCG mineralization preserved in Chile and Peru (e.g., Sillitoe, 2003; Groves et al., 2010; Chen et al., 2013), as well as alkaline porphyry Cu-Au deposits that occur during episodes of extensional rifting within greater Cordilleran -type orogenic events (Mumin et al., 2007, 2010; Richards and Mumin, 2013a,b; Logan and Mihalynuk, 2014; Richards et al., in press).

2. IOCG and IOA DEPOSITS

Polymetallic, IOCG deposits are a favorable exploration target because of their potential to host large tonnages of ore metals, particularly Cu, Fe, Au, and U, as well as accessory Ag, Bi, Co, and rare earth-elements. In addition, IOA deposits can host significant Fe and P resources. Common characteristics of IOCG deposit are structurally controlled mineralization with hydrothermal magnetite and/or specular hematite as a major constituent, less abundant chalcopyrite ± bornite and precious metals, and extensive K ± Si ± Ca-metasomatic haloes (e.g., Hitzman et al., 1992; Sillitoe, 2003; Barton and Johnson, 2004; Dreher, 2008; Richards and Mumin, 2013a). Commonly, the parental mineralizing fluids are highly saline (up to 60% wt.% NaCl equiv.) ± CO_2-rich fluids (e.g., Oreskes and Einaudi, 1992; Huston et al., 1993; Perring et al., 2000; Baker et al., 2008; Somarin and Mumin, 2014). Despite these commonalities, individual deposits are varied in terms of metal budgets, mineralization style, alteration, tectonic setting, age, and nature of the host rocks. The origin of the oxidizing fluids is poorly understood, and as such region-derived models are common for the genesis of these deposits (Fig. 1; Barton and Johnson, 1996; Pollard, 2000; Corriveau et al., 2010b; Groves et al., 2010; Mumin et al., 2010; Smith et al., 2012; Chen et al., 2013; Richards and Mumin, 2013a, b; Acosta-Góngora et al., 2015a,b).

The stable isotope character ($\delta^{18}O$, $\delta^{34}S$, and $\delta^{37}Cl$) of IOCG mineralizing fluids has been used to suggest that they originated as magmatic, evaporitic, formation, metamorphic, and sea-water derived, or as mixtures of some of these end-members (e.g., Oreskes and Einaudi, 1992; Williams, 1994; Pollard, 2000, 2006; Chiaradia et al., 2006; Benavides et al., 2007; Hunt et al., 2007; de Haller and Fontboté, 2009; Gleeson and Smith, 2009). The presence of apparently evaporite-derived fluids in some deposits has been postulated as a key factor for the development of the extensive Ca and Na alteration and complexation of metals in some IOA and IOCG systems (Barton and Johnson, 1996, 2000; Baker et al., 2008; Xavier et al., 2008; Gleeson and Smith, 2009; Barton, 2014). Halogen and noble gas studies from selected IOCGs and IOAs have reinforced the presence of non-magmatic fluid sources in the mineralizing system and the importance of magmatic-derived fluids mixing with non-magmatic fluids, for metal deposition (Chiaradia et al., 2006; Fisher and Kendrick, 2008; Smith et al., 2012). Alternatively, a number of investigators suggest that the alteration and ore minerals in IOCG systems have a magmatic, or dominantly magmatic source, derived from calc-alkaline to moderately alkaline suites similar to the ones responsible for Cu-Au porphyry deposits (Pollard, 2000, 2006; Mumin et al., 2010; Richards and Mumin, 2013a,b). Pollard (2001) further suggests that high levels of CO_2 promote the separation of ore fluids from the crystallizing magma at a wide range of pressures that are compatible with the depths inferred for these systems. Furthermore, CO_2 may also influence the Ca-Na partitioning between silicate melts and fluids, potentially generating brines with high Na/K ratios that might be responsible for the widespread sodic alteration present in many IOCG settings. The generation of iron oxide-dominated systems and the corresponding sodic alteration for some deposits, has also been explained as having been formed by metamorphic processes involving high temperature saline fluids (500 to 600 °C; up to 40% wt.% NaCl equiv.; Williams, 1994). The salinity of these fluids is interpreted to have been acquired from older Cl-rich rocks, and the introduction of metals is the epigenetic with respect to iron-enrichment processes (Williams, 1994).

The Sue-Dianne and the Damp prospects in the Great Bear magmatic zone (Table 1) contain breccias that were recognized to be similar in nature to Olympic Dam breccias (Fig. 2C-D; Gandhi, 1994) and hence-forth were considered as IOCG deposits (Goad et al., 2000). In the Echo Bay region the IOCG model has been used in exploration and to reclassify previously known mineralization and alteration (Corriveau, 2007; Mumin et al., 2007, 2010; Somarin and Mumin, 2014; Mumin et al. 2014). The NICO deposit in the southern Great Bear was recognized by Goad et al. (2000) as an IOCG-like deposit, and this has been supported by detailed mineral deposit and regional alteration studies (Table 1; Acosta-Góngora et al. 2015a, b; Montreuil et al. 2013, 2015). The Fab Lake Cu-U prospect is another example of an IOCG system in the Great Bear (Gandhi 1994; Potter et al. 2013; Mountreuil et al. 2016). Magnetite-apatite ± actinolite mineralization is spatially and potentially genetically associated with the IOCG mineralization and associated alteration throughout the Great Bear magmatic zone (Table 1: Reardon, 1992; Gandhi, 1994; Mumin et al., 2007, 2010). This has also been referred to as Kiruna-type, due to similarities with Fe-oxide apatite deposits at Norrbotten County, Sweden (Hildebrand, 1986; Smith et al., 2012). Type examples occur in the Camsell River area, adjacent to the Terra polymetallic vein deposit (Fig. 2A-B; Badham and Morton, 1976; Hildebrand, 1986) and in the Echo Bay area (Reardon, 1992; Somarin and Mumin, 2014); less-voluminous examples occur throughout the Great Bear magmatic zone as veins, breccia cements, and replacements (Table 1: Gandhi, 1994; Corriveau et al., 2007, 2010b; Mumin et al., 2007, 2010; Potter et al., 2013; Acosta-Góngora et al., 2014).

The Great Bear IOCG and IOA deposits are not only spatially associated (Fig. 1), but the timing of both is now well-constrained between ca. 1873 and 1869 Ma (Fig. 3; Ootes et al., 2010; Acosta-Góngora et al., 2015b; Montreuil et al., 2013, 2016). The IOA mineralization is related to fractionation of intermediate, high-level plutons (Badham and Morton, 1976; Hildebrand, 1986; Reardon, 1992). A link between IOCG mineralization and magmatic-hydrothermal processes is readily apparent from the regional and detailed geological relationships (e.g., Gandhi 1994; Mumin et al. 2014), but is also clearly demonstrated using $\delta^{34}S$ values of the mineralization (Fig. 4; Acosta-Góngora et al., 2015b, accepted with revisions Min Dep). The IOCG-IOA association that is evident in the Great Bear magmatic zone is in direct contrast to the work of many other investigators who have separated these two deposits types due to lack of direct association in most IOCG districts (e.g., Williams, 2010).

3. GEOLOGY

3.1 Regional Overview

The Great Bear magmatic zone is preserved in bedrock exposures over 450 km of north-south strike length and up to 75 km width. It is unconformably covered and obscured to the west by flat lying Paleozoic and Mesozoic sedimentary rocks. An area of low-magnetic response underneath the Phanerozoic platform has been historically considered Hottah terrane, however U-Pb zircon dating of basement cuttings demonstrate this area to be mostly underlain by Great Bear magmatic zone (Ross et al., 2000). To the north it is covered by the <1850 Ma Coppermine Homocline (e.g., Hahn et al., 2013). The Great Bear magmatic zone is a ca. 1875 to 1850 Ma composite plutonic system, with a high ratio of plutonic rocks to volcanic rocks (Fig. 3; Bowring, 1984; Gandhi et al., 2001; Hildebrand et al., 2011b; Ootes et al., 2015). It was constructed on >1895 Ma crust of the Hottah terrane in the north, but was preceded in the south by the <1885 Ma Treasure Lake Group metasedimentary rocks (Figs. 1 and 3; Reichenbach, 1991; Gandhi and van Breemen, 2005; Hildebrand et al., 2010a, b; Davis et al., 2015; Ootes et al., 2015). The eastern limit of the Hottah terrane is demarcated by the north-striking Wopmay fault zone, which is also the western limit of Archean basement rocks in the metamorphic internal zone of Wopmay orogen (Fig. 1; Jackson et al., 2013). This fault truncates Great Bear magmatic zone plutonic suites, and although chronologically equivalent plutons exist to the east, it is challenging to reconstruct the earlier geometry of these plutons across the fault due to a lack of assured piercing points. Consequently, the extent of lateral movement along the Wopmay fault during and after Great Bear magmatism remains unresolved and could be on the order of 10s to >100 km.

3.2 Pre-Great Bear Magmatism: The Hottah Terrane

The basement to the Great Bear is the Hottah terrane (Figs. 1 and 3), and this basement undoubtedly affected the petrological and structural evolution of Great Bear magmatism (e.g., Bowring and Podosek, 1989; Hildebrand et al., 2010; Davis et al., 2015; Ootes et al., 2015). The Hottah terrane is considered to be a 1.93 to 1.89 Ga volcanic arc developed on a >1.95 Ga exotic crustal block, relative to the Archean Slave craton (Hildebrand, 1981; Hildebrand et al., 1987, 2010a; Bowring and Grotzinger, 1992; Davis et al., 2015; Ootes et al., 2015). The Hottah terrane was previously considered to have evolved above a west-dipping subduction zone and subsequently collided with the western Slave craton and Coronation passive margin at ca. 1.88 Ga (Bowring and Grotzinger, 1992; Hildebrand et al., 2010a; Hoffman et al., 2011). More recent advances in bedrock evidence and detrital zircon signatures (Fig. 3) suggest, however, that the Hottah terrane is a vestige of an active margin (arc crust) that evolved adjacent to the Taltson (or Ksituan) magmatic zone, which are preserved to the south of the Slave craton (Davis et al., 2015; Ootes et al., 2015). In this interpretation, the Hottah terrane was juxtaposed to the Slave craton via transtensional shear displacement, initiated during arc rifting at ca. 1.91 Ga; dextral transpressional movement continued until its arrival around ca. 1.88 Ga (Ootes et al., 2015).

Regardless of how the Hottah terrane arrived adjacent to Slave craton, it is relevant that it contains a protracted Paleoproterozoic crustal evolution – including a long-lived ca. 2.0 to 1.96 Ga magmatic arc history culminating at 1.97 Ga (Fig. 3). The evidence for this is only provided by the detrital zircon record, as U-Pb, ε_{Hf}^{T}, and $\delta^{18}O$ values of this phase record continental arc magmatism, potentially represented by the Taltson (or Ksituan) magmatic zone to the south (Davis et al., 2015). The detrital zircon data also point to a parental crust with an older 2.1 to 2.5 Ga Paleoproterozoic history, but with a Neoarchean antiquity (>2.6 Ga), a history very similar to that of the western Rae craton (van Breemen et al., 2013; Card et al., 2014; Davis et al., 2015).

The ca. 1.97 Ga arc magmatism was followed by deposition of <1.95 Ga pelite and metabasalt in the Holly Lake metamorphic complex, determined from a maximum deposition age of detrital zircons (Fig. 3; Davis et al., 2015). This was deformed, metamorphosed and intruded by the Hottah plutonic complex at ca. 1.93 Ga, which was followed by intrusion of compositionally mixed granite-gabbro plutonic phases at ca. 1.91 Ga. These plutonic phases are collectively interpreted to record a return to arc magmatism in the Hottah terrane (Fig. 3; Ootes et al., 2015). This second magmatic event evolved within an extensional environment preserved as the Bell Island Bay Group. This includes basal volcanogenic sandstones that give way to subaerial rhyolite and lesser basalt that erupted at ca. 1.905 Ga, which is overlain by quartz arenite deposited ca. 1.90 Ga, and followed by pillow basalt and lesser rhyodacite erupted at ca. 1.895 Ga (Fig. 3; Ootes et al., 2015). The evidence supports that these arc-like magmatic events were part of a 70 to 100 million year subduction-related evolution, in spite of an incomplete bedrock record (Davis et al., 2015; Ootes et al., 2015).

The oldest exposed bedrock in the southern Great Bear (south of 64^{o}30'N) is a platform-like, shallowing-upward sequence of siltstone, calc-silicate, and quartzite of the Treasure Lake Group (TLG; Fig. 3; Gandhi and van Breemen, 2005; Acosta-Góngora et al., 2015b). Detrital zircon grains constrain the maximum depositional age to <1.885 (Gandhi and van Breemen, 2005; Bennett and Rivers, 2006b) and, therefore, it is younger than the Hottah terrane rocks preserved to the north (Davis et al., 2015; Ootes et al., 2015). The TLG was metamorphosed to lower amphibolite facies prior to or synchronous with early Great Bear magmatism (Fig. 3; Gandhi and van Breemen, 2005). The base of the TLG is not observed and it remains uncertain if it was deposited on Hottah terrane, or Slave craton crust. It was deposited at a similar time as the Recluse Group foredeep sedimentary rocks on the Coronation margin (Hoffman et al., 2011) and parts of the Great Slave Supergroup in the East Arm of Great Slave Lake (Bowring et al., 1984; van Breemen et al., 2013).

3.3 Great Bear Magmatism

3.3.1 Geochronology

A U-Pb zircon crystallization age of 1876.4 ± 2.4 Ma from a rhyolitic ash tuff bed indicates the onset of Great Bear magmatism (Fig. 3; Ootes et al., 2015), supporting previously determined ages (Bowring, 1984; Gandhi et al., 2001; Bennett and Rivers, 2006a). Three stages of volcanism followed: LaBine Group andesitic volcanism at ca. 1873 Ma, Faber rhyolite volcanism and Dumas Group bimodal volcanism at ca. 1869 Ma, and Sloan Group rhyolite and basalt volcanism at ca. 1862 Ma (Fig. 3; Bowring, 1984; Gandhi et al., 2001; Bennett and Rivers, 2006a; Ootes et al., 2015). However, the Great Bear magmatic zone is volumetrically dominated by monzogranitic through monzonitic plutonic phases emplaced between ca. 1873 and 1855 Ma (Fig. 3; Gandhi et al., 2001; Bennett and Rivers, 2006; Hildebrand et al., 2010b; Bennett et al., 2012; Jackson and Ootes, 2012; Ootes et al., 2013; Ootes et al., 2015; Montreuil et al., 2016). The youngest phase of Great Bear magmatism is represented either by rapakivi-textured granitic plutons at ca. 1855 Ma (Fig. 3; Gandhi et al., 2001), or late syenitic intrusions at ca. 1845 Ma that are only rarely preserved and documented (Bowring, 1984). Similar-aged plutons at ca. 1845

Ma are reported from the Fort Simpson terrane in the subsurface of the Phanerozoic platform to the west (Villeneuve et al., 1991).

Great Bear plutonic rocks that predate mineralization appear to be rare, although there is some evidence of ca. 1873 Ma plutonic rocks that contain a penetrative foliation (Gandhi et al., 2001; Bennett and Rivers, 2006a; Jackson, 2008). Where identified, these locally have a distinctive striped appearance (alternating pink and white) on the meter scale, where pink rocks are close to primary igneous compositions; the white zones are characterized by titanite and completely recrystallized silicate minerals, and therefore represent hydrothermal alteration pathways (e.g., see figure 13e, f in Jackson, 2008). This indicates these older phases were extensively altered during younger magmatic/mineralizing phases. The alteration zones associated with the mineralization are spatially extensive (Table 1; Corriveau et al., 2007, 2010; Mumin et al., 2007, 2010; Montreuil et al., 2013, 2015, 2016; Potter et al., 2013; Somarin and Mumin, 2014; Mumin, 2015), and it is possible that other pre-mineralization plutonic rocks existed in the Great Bear magmatic zone, but may have been altered and obscured by younger metasomatic events (Montreuil et al., 2013; Corriveau et al., 2015).

Early stages of metallic mineralization include intrusion-related Cu-Mo-U within tourmaline-biotite veins that cut the Treasure Lake Group (Gandhi, 1994; Ootes et al., 2010). A Re-Os molybdenite date (1873.4 ± 6.1 Ma) and an Ar-Ar biotite date (1875 ± 8 Ma) indicates vein formation and mineralization at that time (Fig. 3; Ootes et al., 2010). South of the NICO Co-Bi-Au deposit, at the southern breccia zone, Re-Os molybdenite dating indicates initial mineralization at 1877 ± 8 Ma (Acosta-Góngora et al., 2015b) and U-Pb zircon dating of an altered felsic dyke at 1873 ± 2 Ma (Fig. 3; Davis et al., 2011) indicates mineralization slightly post-dates the onset of Great Bear volcanism (Fig. 3). Adjacent to the NICO deposit and southern breccia zone, a ca. 1873 Ma leucogranite dyke is overprinted by alteration (Gandhi et al., 2001), providing further maximum age constraints (Fig. 3). The latest stages of mineralization at the NICO deposit yield a Re-Os molybdenite age of 1865 ± 9 Ma (Fig. 3; Acosta-Góngora et al., 2015b). This date could support that the mineralization-related processes continued to ca. 1865 Ma, although the upper bound on the error allows that all mineralization was complete by ca. 1869, consistent with U-Pb zircon dating of cross-cutting plutons and dykes (Fig. 3; Davis et al. 2011). The timing of mineralization has elsewhere been constrained, for example at the FAB IOCG prospect, where U-Pb zircon dating of cross-cutting intrusive phases brackets the Cu-U mineralization to a window between ca. 1870.1 ± 1.7 Ma and 1866.8 ± 1.3 Ma (Montreuil et al., 2016). A hornblende granite and differentiated mafic dyke crystallized at 1866.4 ± 0.6 Ma and 1865.1 ± 0.7 Ma, respectively, and cut previously altered volcanic rocks and hypabyssal porphyry (Bennett et al., 2012). This further provides a minimum age for extensive alteration, which is regionally related to the mineralization processes (Table 1; Montreuil et al., 2013, 2015, 2016).

Plutonic rocks that are interpreted to be synchronous with mineralization, such as the Balachey pluton and Mystery Island and Rainy Lake intrusive suites, are mostly known from northern Wopmay orogen (Hildebrand, 1986; Reardon, 1992; Mumin et al., 2007, 2010; Hildebrand et al., 2010b; Mumin, 2015). These plutons crystallized between ca. 1874 and 1872 Ma (Bowring 1984; Davis et al., 2011). They are heterogeneous, as a result of igneous differentiation and syn-magmatic hydrothermal alteration processes, and are genetically related to extensive IOA veins, plugs, and breccias, and IOCG mineralization (Badham and Morton, 1976; Hildebrand, 1986; Mumin et al., 2007, 2010; Corriveau et al., 2010; Potter et al., 2013; Acosta- Góngora et al., 2014; Somarin and Mumin 2014; Mumin, 2015). In the southern Great Bear magmatic zone, possible syn-mineralization plutons have either not been identified, have not been studied in detail, or are extensively overprinted by alteration systems (e.g., Potter et al., 2013; Somarin and Mumin, 2014). It remains likely that the earliest (>ca. 1869 Ma) components of what Gandhi et al. (2001) refer to as the Marion River batholith are synchronous with mineralization (Bennett and Rivers, 2006; Bennett et al., 2012)

Most of the plutonic rocks in the Great Bear magmatic zone post-date mineralization and crystallized between ca. 1869 and 1855 Ma (Bowring, 1984; Gandhi et al. 2001; Bennett and Rivers, 2006a). These plutons consist of large-scale, coarse-grained intrusions with locally chilled and/or fractionated margins, and were emplaced at high crustal levels (e.g., Jackson, 2008; Hildebrand et al., 2010b; Jackson and Ootes, 2012; Ootes et al., 2013; Montreuil et al., 2016). Equigranular biotite-hornblende granodiorite plutons that occur east of Hottah Lake, crystallized at ca. 1869 Ma, and contain a penetrative foliation that is preserved by the mafic minerals (Fig. 3; Ootes et al., 2015). Volumetrically however, most of the plutonic phases are intruded between ca. 1867 and 1860 Ma, are not penetratively deformed, and consist of equigranular granite to quartz-monzonite, hornblende-monzonite, and coarse-grained K-feldspar porphyritic granite (Bowring, 1984; Gandhi et al., 2001; Hildebrand et al., 2011b; Jackson and

Ootes, 2012). Individual plutons have been given a variety of names across the magmatic zone, but are likely part of a large-scale, long-lived and differentiated batholith (e.g., Gandhi et al., 2001; Jackson, 2008; Hildebrand et al., 2010b; Jackson and Ootes, 2012). The latest pulse of Great Bear magmatism consists of ca. 1860 to 1855 Ma coarse-grained granitic plutons with prevalent rapakivi-texture (Gandhi et al., 2001; Bennett and Rivers, 2006a; Jackson and Ootes, 2012), the distribution of which can be traced both from bedrock mapping and from geophysical signatures (e.g., Hildebrand et al., 2010b; Jackson and Ootes, 2012; Hayward and Corriveau, 2014).

East of the Wopmay fault zone, intrusive rocks that are correlative to the Great Bear plutons include the ca. 1867 Ma Zinto suite, which ranges from granodiorite to gabbro (Bennett and Rivers, 2006a; Jackson, 2008; Jackson and Ootes, 2012; Jackson et al., 2013). These are dominantly equigranular and their composition, age, and deformed nature indicate that these plutons may be correlative to the deformed ca. 1869 Ma biotite-hornblende granodiorite near Hottah Lake and also provide a relative timing for the deformation event that affected those and older documented plutonic phases (Fig. 3; Ootes et al., 2015). The youngest plutons crystallized between ca. 1858 to 1850 Ma (Bowring, 1984; Jackson et al., 2013) and are age-correlative to the late rapakivi-texture plutons that crystallized at ca. 1855 Ma in Great Bear magmatic zone (Gandhi et al., 2001). The rapakivi-textured granites and Bishop intrusive suite mark the end of ca. 150 million years of intermittent and pulsed magmatism related to an evolving continental orogenic belt (Fig. 3; Davis et al., 2015; Ootes et al., 2015).

3.3.2 Geochemistry

The geochemical attributes for the Hottah plutonic complex and Bell Island Bay Group of the Hottah terrane, the basement to the Great Bear magmatic zone, are presented in Reichenbach (1991) and Ootes et al. (2015). In general, the LaBine Group volcanic rocks that erupted pre-to syn-mineralization are extensively altered (e.g., Potter et al., 2013; Mumin, 2015; Montreuil et al., 2016). This includes heterogeneous hydrothermal alteration that is thought to be a result of hydrothermal circulation related to the mineralizing systems (e.g., Mumin et al., 2007, 2010; Corriveau et al., 2010b; Montreuil et al., 2013, 2015, 2016; Potter et al, 2013; Acosta-Góngora et al., 2015b; Corriveau et al., 2015; Mumin, 2015; Montreuil et al., 2016). Due to the extensive nature of the alteration, including potassic metasomatism, only least-altered samples from geochemical datasets (D'Oria, 1998; Azar, 2007; Corriveau et al., 2015; Ootes et al., 2015) are used in Figures 5-8. Least-altered refers to samples that show little to no sign of physical or geochemical change from their original composition. Forty-nine least-altered volcanic samples were identified from across the magmatic zone and include post-mineralization samples from the younger ca. 1860 Ma Sloan Group. Two hundred and thirty one least-altered intrusive samples are from across the Great Bear magmatic zone, and while a few early to syn-mineralization samples are included in the data, the bulk are either late or post-date the mineralizing systems (Figs. 5-8; Table A1). Previously unpublished geochemical data are presented in Table A1A and samples used from previously published studies are presented in Table A1B.

The plutonic samples all range from granite to monzodiorite on a normative QAP plot (Fig. 5A). In terms of high field strength element (HFSE) ratios the volcanic rocks range from basaltic-andesite to rhyolite, which is also the case for the plutonic rocks (Fig 5B). Utilizing the SiO_2 vs K_2O diagram (Pecerrillo and Taylor, 1976) all of the igneous rocks can be considered as high-K calc-alkaline to shoshonitic, although there is significantly more K_2O scatter in the volcanic rocks (Fig. 5C). Potassium metasomatism is ubiquitous throughout the Great Bear magmatic zone and all the samples, even the most mafic end-members, are high in K_2O (Fig. 5C Ootes et al., 2013; Somarin and Mumin, 2013). It is difficult to constrain if the scattered K_2O values (Fig. 5C) are primary or a result of K-metasomatism, and proxy elements and elemental ratios (Müller et al., 1992; Hastie et al., 2007) are utilized later in the discussion to further discriminate the high-K to shoshonitic nature of the igneous rocks. All of the samples share similar chondrite and primitive mantle-normalized rare earth and trace-element patterns, displaying elevated LREE/HREE and Th, negative Nb, P, and Ti, and variable Eu anomalies (Fig. 6). Some notable variation exists; early intrusions have a comparable normalized rare-earth element profile to the volcanic rocks with little to no Eu anomaly. One single Sloan Group rhyolite crystal tuff is more REE-enriched than the other volcanic rocks, with a pronounced negative Eu anomaly (Fig. 6; Ootes et al., 2015), similar in nature to the intrusions that post-date the ca. 1870 Ma mineralizing systems. Strontium anomalies are variably negative in the normalized data, as are the overall abundances of HREE and Y (Fig. 6). Yttrium, which can be considered a proxy for the Ho and HREE, shows a wide spread of values, combined with a low and narrow range of Sr/Y values (Fig. 6D). While Sr can be mobile during alteration, the relatively consistent Sr/Y from the least altered samples supports these are mostly primary Sr values. This suggests that the overall chemistry of the rocks was variably controlled by plagioclase fractionation (Fig. 6D).

A small dataset of Nd and Sr isotopic data is plotted in Figure 8. The most mafic rocks have ε_{Nd} values of +0.9 to -0.9, below depleted mantle values, and the more felsic rocks have compositions only slightly more evolved than the mafic compositions. Possible explanations for this include: 1) the magmas were derivated from a sediment-contaminated subduction zone, which would lower the values in mafic rocks; 2) crustal contamination and assimilation-fractional crystallization (AFC) processes during magma staging and crystallization, or; 3) a combination of the above processes. Rocks with basaltic compositions are relatively rare, and the bulk of the rocks are more felsic in composition. To test the controls on the primary chemistry of the felsic intrusive rocks, we have separated out a suite of samples from a mafic dyke (Figs. 5-7). The dyke is north-striking, predominantly gabbroic in composition, although locally fractionated and co-mingled, cuts previously altered felsic porphyry and volcanic rocks, and is dated at ca. 1866 Ma (Bennett and Rivers, 2006a; Jackson, 2008; Bennett et al., 2012). The gabbroic nature of this dyke is the most primitive of the plutonic rocks, yet shares geochemical attributes with the more felsic rocks (Fig. 6D). Therefore, these are mafic end-members of the granitic and volcanic suites; however, while their isotopic compositions are more juvenile than the felsic rocks, they are still evolved relative to depleted mantle, supporting a subduction modified source, with minor crustal assimilation (Fig. 8). The granitic samples may have derived their more evolved Sr and Nd values from mixing of the parental magma and assimilation of older crust (Figs. 6D and 8), a mixture of the slightly older the Treasure Lake Group sedimentary rocks and phases preserved in the Hottah terrane (Fig. 4).

The trace-element profiles are consistent with arc-related volcanic rocks (Figs. 6 and 7; e.g., Pearce and Norry, 1979; Kelemen et al., 1993; Marschall and Schumacher, 2012). In terms of Y-Nb, all of the samples plot within the volcanic arc – syn-collisional arc and trend to the within-plate zone (Fig. 7A). Samples that plot in the within-plate zone, particularly the late rapakivi-texture samples, may be a result of the aforementioned AFC processes resulting in relatively high Y values, or related to local extension in an overall ‘arc’ environment. Such examples of within-plate geochemical signatures in overall arc environments are not uncommon and record the transition from convergence to extension in convergent margins (e.g., Bryan, 2007). While K-metasomatism is ubiquitous throughout the Great Bear magmatic zone, the high

K_2O values (Fig. 5C) are consistent with the enrichment of other radiogenic elements (U, Th) that are likely primary in the Great Bear igneous rocks (Ootes et al., 2013; Somarin and Mumin, 2013). To help further constrain tectonic affinities, we have plotted relatively immobile elements Co vs. Th, suggested proxies for more mobile SiO_2 and K_2O, respectively (Fig. 8B; Hastie et al., 2007), and trace element ratios (Fig. 7C-D; Müller et al., 1992). The results further support that the Great Bear igneous rocks are predominantly shoshonites (Fig. 7B-D) and by analogy most akin to potassic continental-arc volcanic rocks (Müller et al., 1992; Hastie et al., 2007).

The geochemical data from the plutonic and volcanic rocks do not support an anorogenic setting or continental-rift environment for Great Bear magmatism (Figs. 6-8). The data also indicate that the magmatic rocks are not adakites, and therefore were not melted directly from a young subducted oceanic slab, or related to slab break-off (Fig. 6D; cf. Defant and Drummond, 1990; Richards and Kerrich, 2007). The geochemical data are consistent with magma derivation from a mantle wedge that was enriched by the subduction-addition of pelagic sediments and associated hydrothermal metasomatism (Fig. 7E; e.g., Wang et al., 2006; Marschall and Schumacher, 2012). Mumin et al. (2014) have suggested that the Great Bear IOCG mineralization formed during an intermittent extensional event during the arc magmatism (Mumin et al., 2014). The high K, Th, LILE, and LREE, and U in the igneous rocks could be derived by low degrees of partial melting, generally considered a result of extension (e.g., Wang et al., 2006; Putirka and Busby, 2007; Pe-Piper et al., 2009). This fits with the trend from convergent to within-plate Nb-Y values on Figure 7A, potentially recording the shift from convergence to extension in Great Bear magmatism. If the Great Bear subduction system stalled, it could have driven this lithospheric extension, explaining the overall shoshonitic nature of the magmatic rocks (Fig. 7). The intermediate magmatism associated with mineralization, between ca. 1873 and 1869 Ma is interpreted to record the onset of this extension (e.g., Mumin et al., 2014), which then transitioned to more felsic dominated magmatism that post-dated the main mineralization stage (Fig. 4; e.g., Ootes et al. 2015).

3.4 Post-Great Bear Magmatism

Magmatic rocks that post-date the ca. 1855 Ma Great Bear granites include rare syenites dated at ca. 1845 Ma, and mafic dykes. The mafic dykes include southeast-striking Cleaver dykes and associated sills at Echo Bay at ca. 1740 Ma (Irving et al., 2004), the Western Channel

Diabase dykes and sheets at ca. 1592 Ma (Hamilton and Buchan, 2010), south-striking Mackenzie dykes at ca. 1270 Ma (LeCheminant and Heaman, 1992; Jackson and Ootes, 2012), and a number of northeast-striking Hottah sheets at ca. 780 Ma, part of the Gunbarrel event (Harlan et al., 2003; Sandeman et al., 2014). The Great Bear plutons preserve a brittle-structural overprint after ca. 1850 Ma, in the form of northeast-striking transcurrent faults that dextrally offset all rocks older than the Cleaver mafic dyke swarm (Hildebrand et al., 1987; Hayward and Corriveau, 2015). These faults are part of the large-scale McDonald fault system to the south, which can be traced for ~500 km in the subsurface of the Phanerozoic platform, from Great Slave Lake to the foothills of the Rocky Mountains (Pilkington et al., 2000; Aspler et al., 2003). Other younger and low-temperature events could be related to processes that affected the overlying <1800 Ma Hornby Bay Group and Recluse Group sedimentary rocks, which are preserved to the north, and the Phanerozoic strata, preserved to the west (Miller, 1982; Byron et al., 2009; Hahn et al., 2013; Gandhi et al., 2013).

4. GEOPHYSICS

Lithospheric-scale two-dimensional geophysical experiments have been conducted across the southern and central Great Bear magmatic zone. These include deep-seismic reflection profiling (Cook et al., 1999; Cook and Erdmer, 2005; Oueity and Clowes, 2010), magnetotelluric experiments (Wu et al., 2005; Spratt et al., 2009), and teleseismic data acquisition (Bostock, 1998; Mercier et al., 2008; Snyder et al., 2014). The 2D geophysical data in those studies collectively support that there is a stacked east-dipping lithospheric mantle beneath this region, related to subducted and frozen oceanic crust (e.g., Cook et al., 1999).

Compilation of the geophysical data into a 3D model (Snyder et al., 2014) yields valuable new insights into the stages and geometry of the subduction system (Fig. 9). Receiver functions use short-wavelength (0.2–5 km) P to S phase conversions to estimate depths to major discontinuities in physical properties affecting seismic wave speeds (Bostock, 1998). These receiver functions are typically calculated as a single average at each receiver station. If sufficient earthquakes are recorded and analyzed at multiple azimuths, a three-dimensional cone of phase conversions can be mapped, either as a 3-D cone (Snyder et al., 2014), or opened out into a 2-D plot (Bostock, 1998). Overlapping 3-D cones were used to group similar converted phases and build a common seismic discontinuity surface (Snyder et al., 2014). The model in

Figure 9 is looking towards the north-northwest and down the dip of the "Hottah" seismic discontinuity surface. The Earth's surface is represented by the Slave craton compilation (Stubley, 2005) and seismic discontinuity surfaces include the Moho in green, and surfaces we assign as "Hottah" in light blue, "Great Bear" in purple, a surface that coincides with the Lac de Gras kimberlite field under the Slave craton is blue, and a mid-lithospheric subhorizontal surface in yellow, at about 150 km depth (Snyder et al., 2014). The Moho surface deepens slightly eastward from 35 to 39 km depth. The surface assigned as Hottah dips at 12°NE toward 058° (strike 302°), the lower surface assigned as Great Bear dips 13°E towards 082° (strike 352°). Beneath the city of Yellowknife, the Hottah surface is at 70 km depth with the Great Bear surface at 120 km. At those depths, the Hottah surface coincides with the top of Bostock's (1998) anisotropic (±5%) H discontinuity, which was interpreted as a 10 km-thick subducted oceanic crust. The Great Bear surface coincides with Bostock's (1998) X discontinuity at 135 km depth. Cook and Erdmer (2005) interpreted the H discontinuity to separate a wedge-shaped westernmost Slave lithosphere from the over- and underthust Hottah terrane and the X discontinuity to separate, in turn, a wedge of Hottah terrane from Ft. Simpson lithosphere. The uppermost Precambrian in those areas is covered by the Phanerozoic platform (Figs. 1 and 9). The subsurface has been interpreted as Hottah terrane (e.g., Aspler et al., 2003), but ca. 1875 and 1840 Ma U-Pb zircon dates from subsurface drill-cuttings indicate this area is actually dominated by Great Bear igneous rocks (Ross et al., 2000).

The double stacked, north and north-northwest striking surfaces beneath the Great Bear and Slave craton are best interpreted as stalled subducted slabs (e.g., Cook et al., 1999; Cook and Erdmer, 2005; Wu et al., 2005; Mercier et al., 2008; Oueity and Clowes, 2010; Snyder et al., 2014). We interpret the upper surface as a relic related to the older Hottah arc and the lower related to Great Bear magmatism; both are interpreted to be derived from the cryptic Nahanni terrane oceanic crust (Ootes et al., 2015). Two outcomes of the geophysical model are worth discussing further, the polarities and the orientations of the surfaces. First, the polarities are both east-dipping; there is no evidence of west-dipping subduction. Moresi and Willis (2015) built 4D numerical model simulations (based on Moresi et al., 2014; Betts et al., 2015) to demonstrate the effects of ridge or plateau collision within an evolving subduction zone. In their study, when a 250 to 500 km-diameter ocean plateau is introduced into the subduction zone, the model evolves to a configuration that is geometrically similar to what is observed in the 3D model as shown in

Figure 9. Both demonstrate two subducted slabs with the older, northeast-dipping and shallower slab superimposed on the younger, east-dipping, steeper subduction zone (Figs. 9 and 10). Another, albeit similar tectonic process that could have led to the preserved geometry, is the subduction of a spreading ridge, which can result in the flattening of the subducted slab (Antonijevic et al., 2015). Many Cenozoic Cu porphyry deposits in the Andes are related to the onset of ridge subduction (Rosenbaum et al., 2005), however this style of mineralization is often associated with adakitic magmas (e.g., Rosenbaum et al., 2005; Richards and Mumin, 2013a) and is followed by a quiescence in the associated arc magmatism (Rosenbaum et al., 2005). Neither an adakitic signature nor a hiatus in magmatism is found in the Great Bear magmatic zone. It is not currently possible to test this more thoroughly and other factors require considerations, such as the precise timing of subduction, other potential driving mechanisms such as plume subduction (Betts et al., 2015), and the exact relationships between relatively flat-slab subduction, magmatism, and IOCG mineralization.

The second outcome from the 3D model relates to the surface orientations (Fig. 9). On the surface, the strike of the Great Bear magmatic zone appears to be north-south, but this geometry is visually controlled by the north-south Wopmay fault zone on the east and, in part the Phanerozoic unconformity to the west (Fig. 1). Previous 2D sections (Cook et al., 1999; Cook and Erdmer, 2005), based on surface potential-field (gravity, magnetics) geophysical data sets (e.g., Hoffman, 1988; Aspler et al., 2003) suggested that the preserved subduction zone strikes north and dips east (Hoffman, 1988; Hildebrand et al., 2010a). Figure 9 demonstrates the older Hottah surface of subducted oceanic slab strikes northwest and dips northeast. This geometry would indicate obliquity between the associate arc and the western Slave margin. Card et al. (2014) suggest the Taltson magmatic zone was originally northwest striking. If Hottah terrane evolved as a component of the Taltson magmatic system as suggested by Davis et al. (2015) and Ootes et al. (2015), then the geometry of the upper surface (Fig. 9) could be an artefact of that subduction and collisional process. The younger surface strikes close to north, and the geometry and timing, if subduction corresponds to Great Bear magmatism, correlates exactly with the structural observations from bedrock mapping (Mumin et al., 2007, 2010; Mumin, 2015) and magnetic interpretation (Aspler et al., 2003). Northeast-striking, brittle faults dextrally offset the Great Bear magmatic zone (e.g., Hildebrand et al., 1987). Hayward and Corriveau (2015) use aeromagnetic constraints to restore the geological contacts along these faults; they demonstrated that the Great Bear magmatic zone had a roughly northwest strike prior to this brittle dextral transposition, which taken with the 3D geophysical image would be consistent with the oblique collision model of Hildebrand et al. (1987). This remains speculative, and these geometries (Fig. 9) require further evaluation and consideration within the context of the evolution of the western and southern Paleoproterozoic margins of the Slave craton and western Rae craton.

In the models of Moresi and Willis (2015) and Betts et al. (2015), following plateau collision, a new oceanic slab began subducting behind the accreted plateau (or similar). The time-frame from collision to subduction re-initiation was ca. 40 million years. This model can be used to account for the evolution of Hottah terrane and Great Bear magmatism (Fig. 10). If post-Hottah terrane subduction re-established at ca. 1880 Ma, that would support collision ca. 40 million years earlier, between 1910 and 1930 Ma; the older age is similar to the time of Hottah plutonic suite magmatism, as well as deformation and metamorphism of the Holly Lake metamorphic complex, and the younger age corresponding to initiation of rapid arc rifting and terrane translation (Fig. 4; Ootes et al., 2015). In Figure 9, the upper surface represents the Hottah subduction system, and the lower surface represents the re-establishment of subduction and related to the onset of Great Bear magmatism after ca. 1880 Ma (Fig. 9). Given the orientations of the surfaces, and considering horizontal scales of >250 km, accretionary crust could have arrived well to the south of the Slave craton, and was perhaps responsible for ca. 1930 to 1920 Ma S-type plutonism in the Taltson magmatic zone (Card et al., 2014).

5. PALEOPROTEROZOIC CORDILLERAN-TYPE IOCG and IOA

Iron oxide copper-gold and IOA mineralization in the Great Bear magmatic zone rapidly followed renewed magmatic flare-up at 1876 Ma, the beginning of the final magmatic pulse in a ca. 150 million year old subduction-related system (Fig. 4; Davis et al., 2015; Ootes et al., 2015). Mineralization is related to magmatism, and occurred in a relatively narrow time-window, over a maximum of about 7 million years, from 1873 to 1866 Ma (Figs. 3 and 4). This supports that magmatism and mineralization were related to some dramatic change in the lithosphere. The 3D modeling demonstrates two frozen surfaces, interpreted as remnant oceanic slabs (Fig. 9) and are similar to 4D synthetic modeling of plateau-collision, and subduction re-initiation (Fig. 10; Betts et al., 2015). The Great Bear shoshonitic magmatism and associated mineralization followed this subduction re-initiation and the overall geochemical nature supports magmatism in an extensional environment. We therefore interpret that the Great Bear slab stalled after subduction re-initiation, leading to extension in the suprasubduction zone, initiating low degree partial melts with shoshonitic affinities (Fig. 7). The onset of extension coincides with intermediate magmatism and mineralization (e.g., Hildebrand 1986; Mumin et al. 2014), which transitioned to a more felsic environment, post-dating mineralization after ca. 1866 Ma (Fig. 4; Ootes et al. 2015).

The relationship between magmatism and mineralization in a suprasubduction environment and the spatio-temporal relationship between IOCG and IOA in the Great Bear is reminiscent of Andean IOCG and IOA deposits (Sillitoe, 2003; Barton et al., 2013; Chen et al., 2013; Richards and Mumin 2013a; Richards et al., in press), rather than an intra-cratonic setting implicated for many other Proterozoic IOCG deposits (Groves et al., 2010). The overall extensional environment suggested for Great Bear deposits is particularly reminiscent of the early Cretaceous deposits in the northern Andes (e.g., Sillitoe 2003). Such active margin characteristics are also attributes of many Phanerozoic Cu-Au porphyry deposits, an alkali end-member in porphyry deposits (Müller and Groves, 1993; Wang et al., 2006; Logan and Mihalynuk, 2014). Additional similarities include the alteration assemblages associated with these Cu-Au porphyry deposits, e.g., extensive albititization and magnetite-actinolite-apatite veins and replacements assemblages, and/or skarns, in the host-rocks (e.g., Logan and Mihalynuk, 2014). These Cu-Au porphyry environments are related to active margin extension, in some cases similar to that depicted for the Paleoproterozoic Great Bear (Wang et al., 2006) and others are related to slab tears, which are invoked to account for alkali magmatism (Logan and Mihalynuk, 2014). A key commonality among all of these is the presence of subducted pelagic sediments and associated mantle metasomatism (e.g., Wang et al., 2006; Richards and Mumin, 2013a). Finally, the metal budgets and relationship with metamorphosed and Fe-altered host supracrustal rocks, particularly the NICO deposit (e.g., Acosta-Gongora et al., 2015a,b), as well the high-K nature of associated igneous phases, shares many commonalities with some documented Oligocene post-orogenic skarn deposits (e.g., Nimis et al., 2014). These relations are suggestive that somehow K-rich magmatic rocks, which assimilated portions of older metamorphic basement, should be considered fertile in terms of Fe-rich polymetallic mineralization. This leads to important and ongoing research questions, such as the nature of metal source(s) and process of mobilization and deposition (e.g., Acosta-Gongora et al., 2015a,b; accepted Mineralium Deposita).

The details regarding Great Bear magmatism and mineralization can be used to support the assertion that there is an IOCG-porphyry continuum (Mumin et al., 2010; Richards and Mumin, 2013a,b), and the mineralization preserved in the Paleoproterozoic Great Bear magmatic zone is part of this continuum. Although the Great Bear magmatic zone deposits are not typical of all Proterozoic IOCG deposits (Groves et al., 2010), or at least what is currently known about them, the overall active margin setting is similar to Andean IOCG and IOA deposits, and potentially Mesozoic and Cenozoic Cu-Au porphyry deposits.

ACKNOWLEDGEMENTS

This is a contribution to the Geological Survey of Canada GEM IOCG (ESS contribution 20150397) and the Northwest Territories Geological Survey South Wopmay bedrock mapping project (NTGS contribution #0091). We thank R. Tosdal and D. Weiss for the Nd and Sr isotopic data and B. Kjarsgaard for beneficial comments on a preliminary version of the manuscript. An anonymous reviewer and D. Lentz provided constructive reviews on behalf of the journal.

REFERENCES

Acosta-Góngora, P., Gleeson, S.A., Samson, I.M., Ootes, L., and Corriveau, L, 2014, Trace element geochemistry of magnetite and its relationship to Cu-Bi-Co-Au-Ag-U-W mineralization in the Great Bear magmatic zone, NWT, Canada: Economic Geology, v. 109, 1901-1928.

Acosta-Góngora, P., Gleeson, S.A., Samson, I.M., Ootes, L., and Corriveau, L., 2015a, Mechanisms of gold refining at the Au–Co–Bi± Cu-W iron–oxide dominated NICO deposit, NWT, Canada: Economic Geology, v. 110, p. 291-314.

Acosta-Góngora, P., Gleeson, S.A., Samson, I.M., Corriveau, L., Ootes, L., Taylor, B.E., Creaser, R.A., Muehlenbachs, K., 2015b, The Paleoproterozoic NICO iron-oxide-cobalt-gold-bismuth deposit, Northwest Territories, Canada: evidence from isotope geochemistry and fluid inclusions: Precambrian Research, 268, p. 168-193.

Acosta-Góngora, P, Gleeson, S.A., Samson, I.M., Corriveau, L., Ootes, L., Jackson, S.E., and Taylor, B.E., Constraints on the origin of polymetallic (Cu-Au-Co-Bi-U±Ag) iron-oxide-dominated systems in the Great Bear magmatic zone: Mineralium Deposita

Antonijevic, S.K., Wagner, L.S., Kumar, A., Beck, S.L., Long, M.D., Zandt, G., Taver, H., and Condori, C., 2015, The role of ridges in the formation and longevity of flat slabs: Nature, v. 524, p. 212-215.

Aspler, L.B., Pilkington, M., and Miles, W.F., 2003, Interpretations of Precambrian basement based on recent aeromagnetic data, Mackenzie Valley, Northwest Territories: Geological Survey of Canada, Current Research 2003-C2, 13 p.

Azar, B., 2007, The lithogeochemistry of volcanic and subvolcanic rocks of the FAB lake area, Great Bear Magmatic Zone, Northwest Territories, Canada: Unpublished B.Sc. thesis, University of Toronto, 96 p.

Badham, J.P.N., 1973, Calc-alkaline volcanism and plutonism from the Great Bear batholith, N.W.T.: Canadian Journal of Earth Sciences, v. 10, p. 1319-1328.

Badham, J.P.N., and Morton, R.D., 1976, Magnetite–apatite intrusions and calc-alkaline magmatism, Camsell River, N.W.T.: Canadian Journal of Earth Sciences, v. 13, p. 348-354.

Baker, T., Mustard, R., Fu, B., Williams, P.J., Dong, G., Fisher, L., Mark, G., and Ryan, C.G., 2008, Mixed messages in iron oxide–copper–gold systems of the Cloncurry district, Australia: insights from PIXE analysis of halogens and copper in fluid inclusions: Mineralium Deposita, v. 43, p. 599-608.

Barton, M.D., 2014, Iron oxide (–Cu–Au–REE–P–Ag–U–Co) systems: Treatise on Geochemistry, Second Edition, Volume 13.20, p. 515-541

Barton, M.D., Johnson, D.A., 1996, An evaporitic-source model for igneous-related Fe-oxide(-REE-Cu-Au-U) mineralization: Geology, v. 24, p. 259-262.

Barton, M.D., and Johnson, D.A., 2004, Footprints of Fe-oxide(Cu-Au) systems, SEG 2004: Predictive Mineral Discovery Under Cover: Centre for Global Metallogeny, Special Publication 33, The University of Western Australia, p. 112-116.

Barton, M.D., Johnson, D.A., Kreiner, D.C., and Jensen, E.P., 2013, Vertical zoning and continuity in Fe oxide (-Cu-Au-Ag-Co-U-P-REE) (or 'IOCG') Systems: Cordilleran Insights: 12th SGA Biennial Meeting 2013.,Proceedings, v. 3, p.1348-1351.

Benavides, J., Kyser, T.K., Clark, A.H., and Oates, C.J., 2007, The Mantoverde Iron Oxide-Copper-Gold District, III Región, Chile: The Role of Regionally Derived, Nonmagmatic Fluids in Chalcopyrite Mineralization: Economic Geology, v. 102, p. 415-440.

Bennett, V., and Rivers, T. 2006a, U-Pb ages of zircon primary crystallization and inheritance for magmatic rocks of the southern Wopmay orogen, Northwest Territories: Northwest Territories Geological Survey, NWT Open Report 2006-006, 65 p. Available at www.nwtgeoscience.ca

Bennett, V., and Rivers, T., 2006b, U-Pb ages of detrital zircons from the southern Wopmay orogen, Northwest Territories: Northwest Territories Geological Survey, NWT Open Report 2006-007, 30 p. Available at www.nwtgeoscience.ca

Bennett, V., Rivers, T., and Jackson, V.A., 2012, A compilation of U-Pb zircon primary crystallization and depositional ages from the Paeloproterozoic southern Wopmay orogen, Northwest Territories: Northwest Territories Geological Survey, NWT Open Report 2012-003, 172 p. Available at www.nwtgeoscience.ca

Betts, P.G., Moresi, L., Willis, D., and Miller, M. S., 2015, Geodynamics of oceanic plateau and plume head accretion and their role in Phanerozoic orogenic systems of China: Geoscience Frontiers, v. 6, p. 49-59.

Bostock, M.G., 1998, Seismic stratigraphy and evolution of the Slave province: Journal of Geophysical Research, v. 103, p. 21183-21200.

Bowring, S.A. 1984, U-Pb zircon geochronology of early Proterozoic Wopmay orogen, N.W.T. Canada: an example of rapid crustal evolution: Unpublished Ph.D. thesis, University of Kansas, 148 p.

Bowring, S.A., and Grotzinger, J.P., 1992, Implications of new chronostratigraphy for tectonic evolution of Wopmay orogen, Northwest Canadian Shield: American Journal of Science, v. 292, p. 1-20.

Bowring, S.A., and Podosek, F.A. 1989, Nd isotopic evidence from Wopmay orogen for 2.0–2.4 Ga crust in western North America: Earth and Planetary Science Letters, v. 94, p. 217-230.

Bryan, S., 2007, Silic Large Igneous Provinces: Episodes, v. 30, p. 20-31.

Byron, S.J., Gleeson, S.A., Muehlenbachs, K., Ootes, L., Jackson, V.A., Samson, I.M., 2009, Giant quartz veins in the Great Bear magmatic zone, Northwest Territories, Canada: SGA2009 - The 10th Biennial Meeting of the SGA, Townsville, Australia.

Card, C.D., Bethune, K.M., Davis, W.J., Rayner, N., and Ashton, K.E., 2014, The case for a distinct Taltson orogeny: evidence from northwest Saskatchewan, Canada: Precambrian Research, v. 255, p.245-265.

Chiaradia, M., Banks, D., Cliff, R., Marschik, R., de Haller, A., 2006, Origin of fluids in iron oxide–copper–gold deposits: constraints from δ^{37}Cl, ^{87}Sr/^{86}Sr$_i$ and Cl/Br: Mineralium Deposita, v. 41, p. 565-573.

Chen, H., 2013, External sulphur in IOCG mineralization: implications on definition and classification of the IOCG clan: Ore Geology Reviews, v. 51, p. 74-78.

Chen, H., Cook, D.R., and Baker, M.J., 2013, Mineralization in the Central Andes and the Gondwana Supercontinent breakup: Economic Geology, v. 108, p. 37-44.

Clowes, R.M., Hammer, P.T.C., Fernández-Viejo, G., Welfored, J.K., 2005, Lithospheric structure in northwestern Canada from Lithoprobe seismic refraction and related studies: a synthesis: Canadian Journal of Earth Sciences, v. 42, p. 1277-1293.

Cook, F.A., and Erdmer, P., 2005, An 1800 km cross section of the lithosphere through the northwestern North American plate: lessons from 4.0 billion years of Earth's history: Canadian Journal of Earth Sciences, 42, p. 1295-1311.

Cook, F.A., van der Velden, A., Hall, K.W., and Roberts, B., 1999, Frozen subduction in Canada's Northwest Territories: Lithoprobe deep lithospheric reflection profiling of the western Canadian Shield: Tectonics, **v.** 18, p. 1-24.

Corriveau, L., 2007, Iron oxide copper-gold deposits: a Canadian perspective, *in* Goodfellow, W.D., ed., Mineral Deposits of Canada: Geological Association of Canada, Mineral Deposits Division Special Publication No. 5, p. 307- 328.

Corriveau, L., Ootes, L., Mumin, A.H., Jackson, V., Bennett, V., Cremer, J.-F., Rivard, B., McMartin, I., and Beaudoin, G., 2007, Alteration vectoring to IOCG(U) deposits in frontier volcano-plutonic terrains, Canada, in Milkereit, B., ed., Exploration 07, 5th: Decennial International Conference on Mineral Exploration, Toronto, Canada, Extended Abstracts, p. 1171-1177.

Corriveau, L., Mumin, A.H., and Setterfield, T., 2010a, IOCG environments in Canada: Characteristics, geological vectors to ore and challenges, in Porter, T.M., ed., Hydrothermal Iron Oxide Copper-Gold And Related Deposits: A Global Perspective, Volume 4 - Advances In The Understanding Of IOCG Deposits: Porter Geoscience Consultancy Publishing, Adelaide, p. 311-344.

Corriveau, L., Williams, W., and Mumin, A.H., 2010b, Alteration vectors to IOCG mineralization from uncharted terranes to deposits, in L. Corriveau, L. and A.H. Mumin, A.H., eds., Exploring for iron oxide copper-gold deposits: Canada and global analogues: Geological Association of Canada Short Course Notes 20, p. 89-110.

Corriveau, L., Lauzière, K., Montreuil, J.-F., Potter, E.G., Hanes, R., and Prémont, S., 2015, Dataset of geochemical data from iron oxide alkali-altered mineralizing systems of the Great Bear magmatic zone (NWT): Geological Survey of Canada, Open File 7643, 24 p.

D'Oria, R.-M., 1998, An investigation of the comagmatic signature of the intrusive/extrusive phases of the Faber Lake Rapakivi Suite, Great Bear Magmatic Zone, NWT: Unpublished B.Sc. thesis, University of Western Ontario, 105 p.

Davis, W., Corriveau, L., van Breemen, O., Bleeker, W., Montreuil, J.-F., Potter, E., and Pelleter, E., 2011, Timing of IOCG mineralizing and alteration events with the Great Bear Magmatic Zone: 39th Annual Yellowknife Feocience Forum, Abstracts of Talks and Posters, Northwest Territories Geoscience Office, Yellowknife Geoscience Forum Abstracts Volume 2011.

Davis, W.J., Ootes, L., Newton, L., Jackson, V.A., and Stern, R., 2015, Characterization of the Paleoproterozoic Hottah terrane, Wopmay Orogen using multi-isotopic (U-Pb, Hf and O) detrital zircon analyses: An evaluation of linkages to northwest Laurentian Paleoproterozoic domains: Precambrian Research, v. 269, p. 296-310.

de Haller, A., and Fontboté, L., 2009, The Raúl-Condestable iron oxide copper-gold deposit, Central Coast of Peru: Ore and related hydrothermal alteration, sulfur isotopes, and thermodynamic constraints: Economic Geology, v. 104, p. 35-384.

Defant, M.J., and Drummond, M.S., 1990, Derivation of some modern arc magmas by melting of young subducted lithosphere: Nature, v. 347, p. 662–665.

Dreher, A.M., Xavier, R.P., Taylor, B.E., Martini, S.L., 2008, New geologic, fluid inclusion and stable isotope studies on the controversial Igarapé Bahia Cu–Au deposit, Carajás Province, Brazil: Mineralium Deposita, v. 43, p. 161-184.

Fisher, L.A., and Kendrick, M.A., 2008, Metamorphic fluid origins in the Osborne Fe oxide–Cu–Au deposit, Australia: evidence from noble gases and halogens: Mineralium Deposita, v. 43, p. 483-497.

Gandhi, S.S., 1994, Geological setting and genetic aspects of mineral occurrences in the southern Great Bear magmatic zone, Northwest Territories, *in* Sinclair, W.D. and Richardson, D.G., eds., Studies of Rare-Metal Deposits in the Northwest Territories: Geological Survey of a Canada Bulletin 475, pp. 63-96.

Gandhi, S.S., and van Breemen, O., 2005, SHRIMP U–Pb geochronology of detrital zircons from the Treasure Lake Group – new evidence for Paleoproterozoic collisional tectonics in the southern Hottah terrane, northwestern Canadian Shield: Canadian Journal of Earth Sciences, v. 42, p. 833-845.

Gandhi, S.S., Mortensen, J.K., Prasad, N., and van Breemen, O., 2001, Magmatic evolution of the southern Great Bear continental arc, northwestern Canadian Shield: geochronological constraints: Canadian Journal of Earth Sciences, v. 38, p. 767-785.

Gandhi, S., Potter, E., Fayek, M., 2013, Polymetallic U-Ag veins at Port Radium, Great Bear magmatic zone, Canada: main botryoidal pitchblende stage cuts 1.74 Ga diabase dykes and has REE signatures diagnostic of unconformity-type deposits: Geological Survey of Canada, Open File 7493, 1 sheet.

Gleeson S.A., and Smith M.P., 2009, The sources and evolution of mineralising fluids in iron oxide–copper–gold systems, Norrbotten, Sweden: constraints from Br/Cl ratios and stable Cl isotopes of fluid inclusion leachates: Geochimica et Cosmochimica Acta, v. 73, p. 5658-5672.

Goad, R.E., Mumin, A.H., Duke, N.A., Neale, K.L., Mulligan, D.L., and Camier, W.J., 2000, The NICO and Sue-Dianne Proterozoic, iron oxide-hosted, polymetallic deposits, Northwest Territories: application of the Olympic Dam model in exploration: Exploration and Mining Geology, v. 9, p. 123-140.

Gorton, M.P., and Schandl, E.S., 2000, From continents to island arcs: A geochemical index of tectonic setting for arc-related and within-plate felsic to intermediate volcanic rocks: The Canadian Mineralogist, v. 38, p. 1065-1073.

Hahn, K., Rainbird, R., and Cousens, B., 2013, Sequence stratigraphy, provenance, C and O isotopic composition, and correlation of the Paleoproterozoic-early Mesorproterozoic upper Hornby Bay and lower Dismal Lake groups, NWT and Nunavut: Precambrian Research, v. 232, p. 209-228.

Hamilton, M.A., and Buchan, K.L., 2010, U–Pb geochronology of the Western Channel diabase, northwestern Laurentia: Implications for a large 1.59 Ga magmatic province, Laurentia's APWP and paleocontinental reconstructions of Laurentia, Baltica and Gawler craton of southern Australia: Precambrian Research, v. 183, p. 463-473.

Harlan, S.S., Heaman, L.M., LeCheminant, A.N., and Premo, W.R., 2003, Gunbarrel mafic magmatic event: A key 780 Ma time marker for Rodinia plate reconstructions: Geology, v. 31, p. 1053-1056.

Hayward, N., and Corriveau, L., 2014, Fault reconstructions using aeromagnetic data in the Great Bear magmatic zone, Northwest Territories, Canada: Canadian Journal of Earth Sciences, v. 51, p. 927-942.

Hastie, A.R., Kerr, A.C., Pearce, J.A., and Mitchell, S.F., 2007, Classification of altered volcanic island arc rocks using immobile trace elements: development of the Th-Co discrimination diagram: Journal of Petrology, v. 48, p. 2341-2357.

Hildebrand, R.S., 1981, Early Proterozoic LaBine Group of Wopmay orogen: remnant of a continental volcanic arc developed during oblique convergence, *in* Campbell. F.HA, ed., Proterozoic Basins of Canada: Geological Survey of Canada, Paper 81-10, p. 133-156.

Hildebrand, R.S., Hoffman, P.F., and Bowring, S.A., 1987, Tectonomagmatic evolution of the 1.9 Ga Great Bear magmatic zone, Wopmay orogen, northwestern Canada: Journal of Volcanology and Geothermal Research, v. 32, p. 99-118.

Hildebrand, R.S., Hoffman, P.F., and Bowring, S.A., 2010a, The Calderian orogeny in Wopmay orogen (1.9 Ga), northwestern Canadian Shield: Geological Society of America Bulletin, v. 122, p. 794-814.

Hildebrand, R.S., Hoffman, P.F., Housh, T., and Bowring, S.A. 2010b, The nature of volcano-plutonic relations and the shapes of epizonal plutons of continental arcs as revealed in the Great Bear magmatic zone, northwestern Canada: Geosphere, v. 6, p. 812-839.

Hitzman, M.W., Oreskes, N., and Einaudi, M.T., 1992, Geological characteristics and tectonic setting of Proterozoic iron oxide (Cu-U-Au-REE) deposits: Precambrian Research, v. 58, p. 241-287.

Hoffman, P.F., Bowring, S.A., Buchwaldt, R., and Hildebrand, R.S. 2011, Birthdate for the Coronation paleocean: age of initial rifting in Wopmay orogen, Canada: Canadian Journal of Earth Sciences, v. 48, p. 281-293.

Hunt, J.A., Baker, T., and Thorkelson, 2007, A review of iron oxide copper-gold deposits, with focus on the Wernecke Breccias, Yukon, Canada, as an example of a non-magmatic end member and implications for IOCG genesis and classification: Exploration and Mining Geology, v. 16, p. 209-232.

Huston, D., Bolger, C., and Cozens, G., 1993, A comparison of mineral deposits at the Gecko and White Devil deposits; implications for ore genesis in the Tennant Creek District, Northern Territory, Australia: Economic Geology, v. 88, p. 1198-1225.

Irving, E., Baker, J., Hamilton, M., and Wynne, P.J., 2004, Early Proterozoic geomagnetic field in western Laurentia: implications for paleolatitudes, local rotations and stratigraphy: Precambrian Research, v. 129, p. 251-270.

Jackson, V.A., 2008, Preliminary geologic map of part of the southern Wopmay orogen (parts of NTS 86B and 86C; 2007 updates); descriptive notes to accompany 1:100,000 scale map: Northwest Territories Geological Survey, NWT Open Report 2008-007, 53 p., 1 map, scale 1:100 000. www.nwtgeoscience.ca

Jackson, V.A., and Ootes, L., 2012, Preliminary geologic map of the south-central Wopmay orogen (parts of NTS 86B, 86C, and 86D); results from 2009 to 2011: Northwest Territories Geological Survey, NWT Open Report 2012-004, 1 map, scale 1:100 000. www.nwtgeoscience.ca

Jackson, V.A., van Breemen, O., Ootes, L., Bleeker, W., Bennett, V., Davis, W.J., Ketchum, J., and Smar, L., 2013, U-Pb zircon ages and field relationships of Archean basement and Paleoproterozoic intrusions, south-central Wopmay Orogen, NWT: implications for tectonic assignments: Canadian Journal of Earth Sciences, v. 50, p. 979-1006.

Kelemen, P.B., Shimizu, N., and Dunn, T., 1993, Relative depletion of niobium in some arc magmas and the continental crust: partitioning of K, Nb, La and Ce during melt/rock reaction in the upper mantle: Earth and Planetary Science Letters, v. 120, p. 111-134.

LeCheminant, A.N., and Heaman, L.M., 1989, Mackenzie igneous events, Canada: Middle Proterozoic hotspot magmatism associated with ocean opening: Earth and Planetary Science Letters, v, 96, p. 38-48.

Logan, J.M., and Mihalynuk, M.G., 2014, Tectonic controls on Early Mesozoic paired alkaline porphyry deposit belts (Cu-Au ± Ag-Pt-Pd-Mo) within the Canadian Cordillera: Economic Geology, v. 109, p. 827-858.

Marschall, H.R., and Schumacher, J.C., 2012, Arc magmas sourced from mélange diapirs in subduction zones: Nature Geoscience, v. 5, p. 862-867.

McMartin, I., Corriveau, L., and Baudoin, G., 2011, An orientation study of the heavy mineral signature of the NICO Co-Au-Bi deposit, Great Bear magmatic zone, NW Territories, Canada: Geochemistry: Exploration, Environment, Analysis, v. 11, p. 293-307.

Mercier, J.-P., Bostock, M.G., Audet, P., Gaherty, J.B., Garnero, E.J., and Revenaugh, J., 2008, The teleseismic signature of fossil subduction: Northwestern Canada: Journal of Geophysical Research, v. 113, B04308, doi:10.1029/2007JB005127.

Miller, R.G., 1982, The geochronology of uranium deposits in the Great Bear batholith Northwest Territories: Canadian Journal of Earth Sciences, v. 19, p. 1428–1448.

Montreuil, J.-F., Corriveau, L., and Grunsky, E.C., 2013, Compositional data analysis of hydrothermal alternations in IOCG systems, Great Bear magmatic zone, Canada: to each alteration types its own geochemical signature: Geochemistry: Exploration, Environment, Analysis, v. 13, p. 229-247.

Montreuil, J.-F., Corriveau, L., and Potter, E.G., 2015, Formation of albitite-hosted uranium within IOCG systems: the Southern Breccia, Great Bear magmatic zone, Northwest Territories, Canada: Mineralium Deposita, v. 50, p. 293-325.

Montreuil, J.-F., Potter, E.G., and Davis, W.J., 2016, Element mobility patterns in magnetite-group IOCG systems: the FAB IOCG system, Northwest Territories, Canada: Ore Geology Reviews, v. 72, p. 562-584.

Montreuil, J.-F., Corriveau, L., and Potter, E.G., De Toni, A., On the relation between alteration facies and metal endowment of iron oxide-alkali-altered systems, southern Great Bear magmatic zone (Canada): Economic Geology, in press.

Moresi, L., and Willis, D., 2015, Time dependent behavior of congested subduction: Elements, v. 11, online content only, 5 movies. http://www.elementsmagazine.org/supplements/e11_2_TOC_Supplements.htm

Moresi, L., Betts, P.G., Miller, M.S., and Cayley, R.A., 2014, Dynamics of continental accretion: Nature, 508, p. 245-248. doi:10.1038/nature13033.

Müller, D., and Groves, D.I., 1993, Direct and indirect associations between potassic igneous rocks, shoshonites and gold-copper deposits: Ore Geology Reviews, v. 8, p. 383-406.

Müller, D, Rock, N.M.S., and D.I. Groves, D., 1992, Geochemical discrimination between shoshonitic and potassic rocks in different tectonic settings: a pilot study: Mineralogy and Petrology, v. 46, p. 259-289.

Mumin, A.H., 2015, Echo Bay IOCG thematic map series: geology, structure and hydrothermal alteration of a stratovolcano complex, Northwest Territories, Canada: Geological Survey of Canada, Open File 7807, 19 p. (18 sheets).

Mumin, A.H., Corriveau, L., Somarin, A.K., and Ootes, L., 2007, Iron oxide copper-gold-type polymetallic mineralization in the Contact Lake Belt, Great Bear Magmatic Zone, Northwest Territories, Canada: Exploration and Mining Geology, v. 16, p. 187-208.

Mumin, H., Somarin, A., Jones, B., Corriveau, L., Ootes, L., and Camier, J., 2010, The IOCG – porphyry – epithermal continuum in the Great Bear magmatic zone, Northwest Territories, Canada, *in* Corriveau, L. and Mumin, A.H., eds., Exploring for Iron Oxide Copper-Gold Deposits: Geological Association of Canada, Short Course Notes 20, p. 57-75.

Mumin, A.H., Phillips, A., Katsuragi, C.J., Mumin, A., and Ivanov, G., 2014, Geotectonic interpretation of the Echo Bay stratovolcano complex, Northern Great Bear Magmatic Zone, Northwest Territories: Northwest Territories Geological Survey, Open File 2014-04, 25 p. www.nwtgeoscience.ca

Nimis, P., Dalla Costa, L., and Guastoni, A., 2014, Cobaltite-rich mineralization in the iron skarn deposit of Traversella (Western Alps, Italy): Mineralogical Magazine, v. 78, p. 11-27.

Ootes, L., Goff, S., Jackson, V., Gleeson, S., Creaser, R., Samson, I.M., Evensen, N., Corriveau, L., and Mumin, H., 2010, Timing and thermochemical constraints on multi-element mineralization at the Nori/RA Cu-Mo-U prospect, Great Bear magmatic zone, Northwest Territories, Canada: Mineralium Deposita, v. 45, p. 549-566.

Ootes, L., Harris, J., Jackson, V.A., Azar, B., and Corriveau, L., 2013, Uranium-enriched bedrock in the central Wopmay orogen: implications for uranium mineralization: Exploration and Mining Geology, v. 21, p. 85-103.

Ootes, L., Davis, W.J., Jackson, V.A., and van Breemen, O., 2015, Chronostratigraphy of the Hottah terrane and Great Bear magmatic zone of Wopmay orogen, Canada, and exploration of a terrane translation model: Canadian Journal of Earth Sciences, v. 52, p. 1-31.

Oreskes, N., and Einaudi, M.T., 1992, Origin of hydrothermal fluids at Olympic Dam; preliminary results from fluid inclusions and stable isotopes: Economic Geology, v. 87, p. 64-90.

Oueity, J., and Clowes, R.M., 2010, Paleoproterozoic subduction in northwestern Canada from near-vertical and wide-angle seismic reflection data: Canadian Journal of Earth Sciences, v. 47, p. 35-52.

Pe-Piper, G., Piper, D.J.W., Koukouvelas, I., Dolansky, L.M., and Kokkalas, S., 2009, Post-orogenic shoshonitic rocks and their origin by melting underplated basalts: the Miocene of Limnos, Greece: Geological Society of America Bulletin, v. 121, p. 39-54.

Pearce, J.A., 1996, A user's guide to basalt discrimination diagrams, *in* Wyman, D.A., ed., Trace Element Geochemistry of Volcanic Rocks; Applications for Massive Sulphide Exploration: Geological Association of Canada, Short Course Notes Volume 12, pp. 79-113.

Pearce, J.A., and Norry, M.J., 1979, Petrogenetic implications of Ti, Zr, Y, and Nb variations in volcanic rocks: Contributions to Mineralogy and Petrology, v. 69, p. 33-47.

Pearce, J.A., Harris, N.B.W., and Tindle, A.G., 1984, Trace element discrimination diagrams for the tectonic interpretation of granitic rocks: Journal of Petrology, v. 25, p. 956-983.

Peccerillo, A., and Taylor, S.R., 1976, Geochemistry of Eocene calc-alkaline volcanic rocks from the Kastamonu area, Northern Turkey: Contributions to Mineralogy and Petrology, v. 58, p. 63-81.

Perring, C.S., Pollard, P.J., Dong, G., Nunn, A.J., and Blake, K.L., 2000, The Lightning Creek Sill Complex, Cloncurry District, Northwest Queensland: a source of fluids for Fe Oxide Cu-Au mineralization and sodic-calcic alteration: Economic Geology, v. 95, p. 1067-1089.

Pilkington, M., Miles, W.F., Ross, G.M., and Roest, W.R. 2000, Potential-field signatures of buried Precambrian basement in the Western Canada Sedimentary Basin: Canadian Journal of Earth Sciences, v. 37, p. 1453-1471.

Plank, T., and Langmuir, C.H., 1998, The chemical composition of subducting sediment and its consequences for the crust and mantle: Chemical Geology, v. 145, p. 325-394.

Pollard, P.J., 2000, Evidence of a magmatic fluid and metal source for Fe-oxide Cu–Au mineralization, *in* T.M. Porter, ed., Hydrothermal Iron Oxide Copper–Gold And Related Deposits: A Global Perspective, Volume 1, Porter Geosciences Consultancy, Adelaide, p. 27-41.

Pollard, P.J., 2001, Sodic (-calcic) alteration in Fe-oxide Cu–Au districts: an origin via unmixing of magmatic $H2O–CO2–NaCl \pm CaCl2–KCl$ fluids: Mineralium Deposita, v. 36, p. 93-100.

Pollard, P.J., 2006, An intrusion-related origin for Cu-Au mineralization in iron oxide-copper-gold (IOCG) provinces: Mineralium Deposita, v. 41, p. 179-187.

Potter, E.G., Montreuil, J-F., Corriveau, L., DeToni, A., 2013, Geology and hydrothermal alteration of the Fab lake region, Northwest Territories: Geological Survey of Canada, Open File 7339, 26 p.

Putirka, K., and Busby, C.J., 2007, The tectonic significance of high-K_2O volcanism in the Sierra Nevada, California: Geology, v. 35, p. 923-926.

Reardon, N.C., 1992, Magmatic-hydrothermal systems and associated magnetite-apatite-actinolite deposits, Echo Bay, Northwest Territories: Unpublished M.Sc. thesis, University of Ottawa, 154 p.

Richards, J.P., and Kerrich, R., 2007, Adakite-like rocks: their diverse origins and questionable role in metallogenesis: Economic Geology, v. 102, p. 537-576.

Richards, J.P., and Mumin, A.H., 2013a, Lithospheric fertilization and mineralization by arc magmas: genetic links and secular differences between porphyry copper ± molybdenum ± gold and magmatic-hydrothermal iron oxide copper-gold deposits: Society of Economic Geology Special Publication 17, p. 277-299.

Richards, J.P., and Mumin, A.H., 2013b, Magmatic-hydrothermal processes within an evolving Earth: iron oxide-copper gold and porphyry Cu ± Mo ± Au deposits: Geology, v. 41, p. 767-770.

Richards, J.P., López, G.P., Zhu, J.-j., Creaser, R.A., Locock, A.J., and Mumin, A.H., Contrasting magmas related to porphyry and iron oxide-copper-gold deposits in Chile: Economic Geology, in press.

Rosenbaum, G., Giles, D., Saxon, M., Betts, P.G., Weinberg, R.F., and Duboz, 2005, Subduction of the Nazca Ridge and the Inca Plateau: insights into the formation of ore deposits in Peru: Earth and Planetary Science Letters, v. 239, p. 18-32.

Ross, G., Annell, H.C., and Hamilton, M.A., 2000, Lithology and U-Pb geochronology of shallow basement along the SNORCLE line, southwest Northwest Territories: A Preliminary Report: SNORCLE Lithoprobe transect workshop, Calgary, AB, 5 p.

Sandeman, H.A., Ootes, L., Cousens, B., and Killian, T., 2014, Petrogenesis of Gunbarrel magmatic rocks: homogeneous continental tholeiites associated with extension and rifting of Neoproterozoic Laurentia; Precambrian Research, v. 252, p. 166-179.

Sillitoe, R.H., 2003, Iron oxide-copper-gold deposits: an Andean view: Mineralium Deposita, v. 38, p. 787-812.

Smith, M.P., Gleeson, S.A., and Yardley, B.W.D., 2012, Hydrothermal fluid evolution and metal transport in the Kiruna District, Sweden: Contrasting metal behavior in aqueous and aqueous–carbonic brines: Geochemica et Cosmochimica Acta, v. 102, p. 89-112.

Spratt, J.E., Jones, A.G., Jackson, V.A., Collins, L., and Avdeeva, A., 2009, Lithospheric geometry of the Wopmay orogen from a Slave craton to Bear Province magnetotelluric transect: Journal of Geophysical Research, v. 114: B01101.

Snyder, D.B., Hillier, M.J., Kjarsgaard, B.A., de Kemp E.A., and Craven, J.A., 2014, Lithospheric architecture of the Slave craton, northwest Canada, as determined from an interdisciplinary 3-D model: G3: Geochemistry, Geophysics, Geosystems, v. 15, doi: 10.1002/2013GC005168.

Somarin, A.K., and Mumin, A.H., 2012, The Paleo-Proterozoic high heat production Richardson granite, Great Bear magmatic zone, Northwest Territories, Canada: source of U for Port Radium?: Resource Geology, v. 62, p. 227-242.

Somarin, A.K., and Mumin, A.H., 2014, P-T composition and evolution of paleofluids in the Paleoproterozoic Mag Hill IOCG system, Contact Lake belt, Northwest Territories: Mineralium Deposita, v. 49, p. 199-215.

Sun, S.S., and McDonough, W.F., 1989, Chemical and isotopic systematics of oceanic basalts: implications for mantle composition and processes, *in* Saunders, A.D., and Norry, M.J., eds., Magmatism in the Ocean Basins: Geological Society of London, Special Publication, 42, p. 313-345.

van Breemen, O., Kjarsgaard, B.A., Tella, S., Lemkow, D., Aspler, L., 2013, U-Pb detrital zircon geochronology of clastic sedimentary rocks of the Paleoproterozoic Nonacho and East Arm basins, Thaidene Nene MERA study area , in D.F. Wright, E.J. Ambrose, D. Lemkow, and G. Bonham-Carter (eds.), Mineral and Energy Resource Assessment of the proposed Thaidene Nene National Park Reserve in the area of the east arm of Great Slave Lake, Northwest Territories: Geological Survey of Canada, Open File 7196, p. 119-142.

Villeneuve, M.E., Thériault, R.J., and Ross, G.M., 1991, U-Pb ages and Sm-Nd signature of two subsurface granites from the Fort Simpson magnetic high, northwest Canada: Canadian Journal of Earth Sciences, v. 28, p. 1003-1008.

Wang, Q., Wyman, D.A., Xu, J.-F., Zhao, Z.-H., Jian, P., Xiong, X.-L., Bao, Z.-W., Li, C.F., and Bai, Z.H., 2006, Petrogenesis of Cretaceous adakitic and shoshonitic igneous rocks in the Luzong area, Anhui Province (eastern China): Implications for geodynamics and Cu–Au mineralization: Lithos, v. 89, p. 424-446.

Williams, P.J., 1994, Iron mobility during synmetamorphic alteration in the Selwyn Range area, NW Queensland; implications for the origin of ironstone-hosted Au-Cu deposits: Mineralium Deposita, v. 29, p. 250-260.

Williams, P.J. 2010, Classifying IOCG deposits, *in* Corriveau, L. and Mumin, A.H., eds., Exploring for Iron Oxide Copper-Gold Deposits: Geological Association of Canada, Short Course Notes 20, p. 13-22.

Williams, P.J., Barton, M.D., Johnson, D.A., Fontbote, L., de Haller, A., Mark, G., Oliver, N.H.S., and Marschik, R., 2005, Iron oxide copper-gold deposits; geology, space-time distribution, and possible modes of origin: Economic Geology 100th Anniversary Volume, p. 371-406.

Wu, X., Ferguson, I.J., and Jones, A.G., 2005, Geoelectric structure of the Proterozoic Wopmay Orogen and adjacent terranes, Northwest Territories, Canada: Canadian Journal of Earth Sciences, v. 42, p. 955-981.

Xavier, R.P., Wiedenbeck, M., Trumbull, R.B., Dreher, A.M., Monteiro, L.V.S., Rhede, D., de Araújo, C.E.G., Torresi, I., 2008, Tourmaline B-isotopes fingerprint marine evaporites as the source of high-salinity ore fluids in iron oxide copper-gold deposits, Carajás Mineral Province (Brazil): Geology, v. 39, p. 743-746.

Figure Captions

Figure 1. Geology of the Great Bear magmatic zone with key areas and mineral deposits discussed in the text and Table 1 identified. Modified after Ootes et al. (2010) and Acosta-Góngora et al. (2014, 2015a, b).

Figure 2. Examples of IOA (Kiruna-type) and IOCG mineralization in the Great Bear magmatic zone. A) magnetite-apatite-actinolite (Mgt-Ap-Act) body adjacent to the Terra five-element vein deposit and B) magnetite (grey) –apatite (pink) veins replacing bedding in the Terra Formation adjacent to the Terra deposit, Camsell River district. C) Hematite (Hem) -cemented breccia with uranium-related staining (U) indicating uraninite mineralization, DAMP Cu-U IOCG prospect. D) Magnetite-cemented breccia associated with the Sue-Dianne Cu-Ag IOCG deposit.

Figure 3. $\delta^{34}S$ data from the Treasure Lake Group (TLG), the host-rocks to the NICO deposit as well as a number of other IOCG deposits and prospects in the Great Bear magmatic zone, compared with $\delta^{34}S$ data from IOCG deposits from other districts. The Great Bear data is consistent with magmatic-derived sulfur in the deposits (modified from Acosta-Góngora et al., 2015, in review, and references therein).

Figure 4. Time-line demonstrating the evolution of the Great Bear magmatic zone and its basement rocks of the Hottah terrane, as well as the tight time-window of IOCG and Kiruna-type mineralization. The Holy Lake metamorphic complex detrital zircon probability histogram is shown to demonstrate the antiquity of the Hottah terranes source environment (modified after Davis et al., 2015). Data for constructing the timeline are from Bowring (1984), Gandhi et al. (2001), Gandhi and van Breemen (2005), Bennett and Rivers (2006a, b), Davis et al. (2011, 2015), Ootes et al. (2015), and Montreuil et al. (2016).

Figure 5. Geochemical discrimination diagrams of Great Bear magmatic zone volcanic and plutonic rocks. A) Quartz-Aklaline-Plagioclase (QAP) normative plot for intrusive rocks. B) High field strength ratio plot (Pearce, 1996) demonstrating a range of primary compositions from basalt through rhyolite; intrusive rock symbols are subdued. C) SiO_2 (wt. %) versus K_20 (w.t %; Pecerrillo and Taylor, 1976) demonstrating their high-K calc-alkaline nature through a range of compositions; intrusive rock symbols are subdued. Data plotted are from least-altered samples in D'Oria (1998), Azar (2007), Corriveau et al. (2015), Ootes et al. (2015), and this study (Supplementary Table A1). The mafic-intermediate samples were selected from various locations across a single differentiated dyke that is up to 30 m wide (Jackson, 2008). Age controls are from Bowring (1984), Gandhi et al. (2001), Bennett and Rivers (2006a), and Ootes et al. (2015).

Figure 6. Normalized rare-earth element (chondrites) and extended trace-element plots (primitive mantle; normalizing values are from Sun and McDonough, 1989) for A) least-altered Great Bear volcanic rocks, B) least-altered Great Bear plutonic rocks, C) mafic-intermediate dyke. D) Sr/Y versus Y plot, modified after Defant and Drummond (1990) and Richards and Kerrich (2007).

Figure 7. Discrimination diagram for A) granitic rocks (Pearce et al., 1984); volcanic rocks are plotted but subdued, and B) volcanic rocks (Hastie et al., 2007); plutonic rocks are plotted but subdued. Symbols in A and B as in Figure 5. Discrimination diagrams B) and C) from Müller et al. (1992). The active continental margin field for felsic to intermediate rocks (shaded grey) is from Gorton and Schandl (2000). Rocks that do not meet the major element criteria (circles), as set out in Müller et al. (1992), are subdued and included for demonstration purposes. E) Trace element ratios demonstrating the geochemical relationship between Great Bear plutonic and volcanic rocks and arc volcanic rocks and global subducted sediment (GLOSS; Plank and Langmuir, 1998). Modified after Marschall and Schumacher (2012).

Figure 8. $^{87}Sr/^{86}Sr_i$ vs. $\varepsilon_{Nd}{}^{T}$ for samples from Great Bear magmatic zone. Approximate MORB values at ca. 1870 Ma are also shown. Symbols as in Figure 5, data in Table A2.

Figure 9. Perspective view of the 3D model of the Slave craton and Wopmay orogen. View is looking from the south-southeast and perpendicular to the dip of the “Hottah” seismic discontinuity surface. The Earth’s surface is represented by the Archean Slave craton (lightest blue), the Archean to Paleoproterozoic Coronation margin (not filled), the Paleoproterozoic Hottah terrane and Great Bear magmatic zone (green), and the Phanerozoic cover (grey). Seismic discontinuity surfaces include the Moho, Hottah, Great Bear, and a surface that coincides with the Lac de Gras kimberlite field in dark blue. The Hottah and Great Bear surfaces are interpreted as the top of relic subducted oceanic slabs. White cones are example receiver functions beneath seismic stations at the Jericho and Sulky Lake (Dharma) kimberlite sites. Blue dots at the surface indicate the location of other seismic sites used to construct 3-D receiver function cones that constrain the four seismic discontinuity surfaces shown. See Snyder et al. (2014) for further description of the construction of these features and uncertainties associated with each. Communities of Gameti, Kugluktuk, and Yellowknife (YK), as well as diamond mines Ekati/Diavik and Gahcho Kue are labeled for reference. View is looking north.

Figure 10. Schematic diagram of 4D model results from introducing a 250 to 500 km wide ocean plateau (black) into a subduction zone. Modified after Betts et al. (2014) to show the possible evolution of the Hottah slab and Great Bear slab in relation to Paleoproterozoic time. The final geometry appears similar to the 3D geophysical modeling demonstrated in Figure 9. See text for discussion.

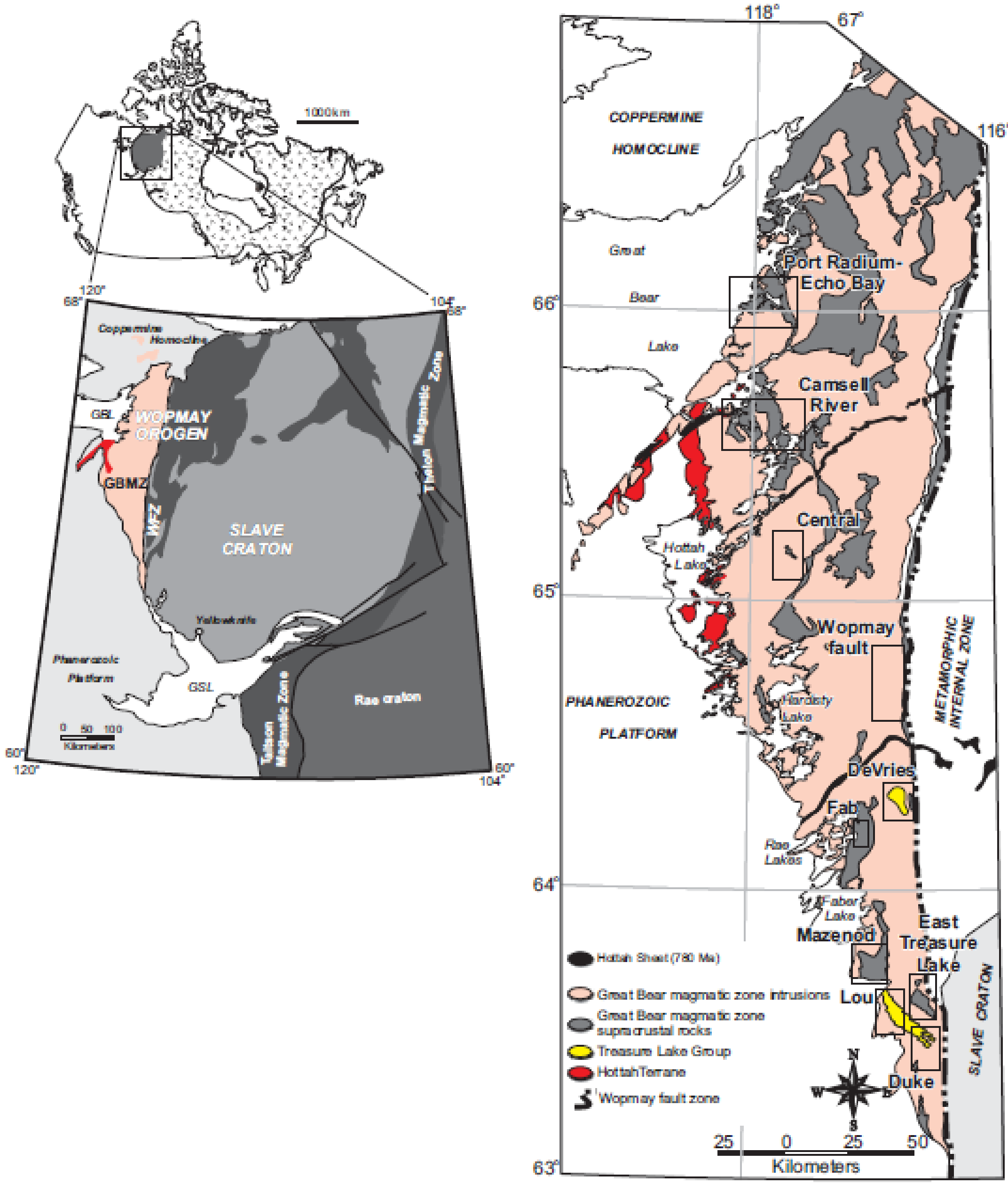
1000km
WOPMAY OROGEN
GBL
GBMZ
WFZ
SLAVE CRATON
Thelon Magmatic Zone
Yellowknife
Phanerozoic Platform
GSL
Taltson Magmatic Zone
Rae craton
0 50 100
Kilometers
COPPERMINE HOMOCLINE
Great Bear Lake
Port Radium-Echo Bay
Camsell River
Central
Hottah Lake
Wopmay fault
METAMORPHIC INTERNAL ZONE
PHANEROZOIC PLATFORM
Hardisty Lake
DeVries
Fab
Rae Lakes
Faber Lake
Mazenod
East Treasure Lake
Lou
Duke
SLAVE CRATON
Hottah Sheet (780 Ma)
Great Bear magmatic zone intrusions
Great Bear magmatic zone supracrustal rocks
Treasure Lake Group
Hottah Terrane
Wopmay fault zone
25 0 25 50
Kilometers

Figure 1

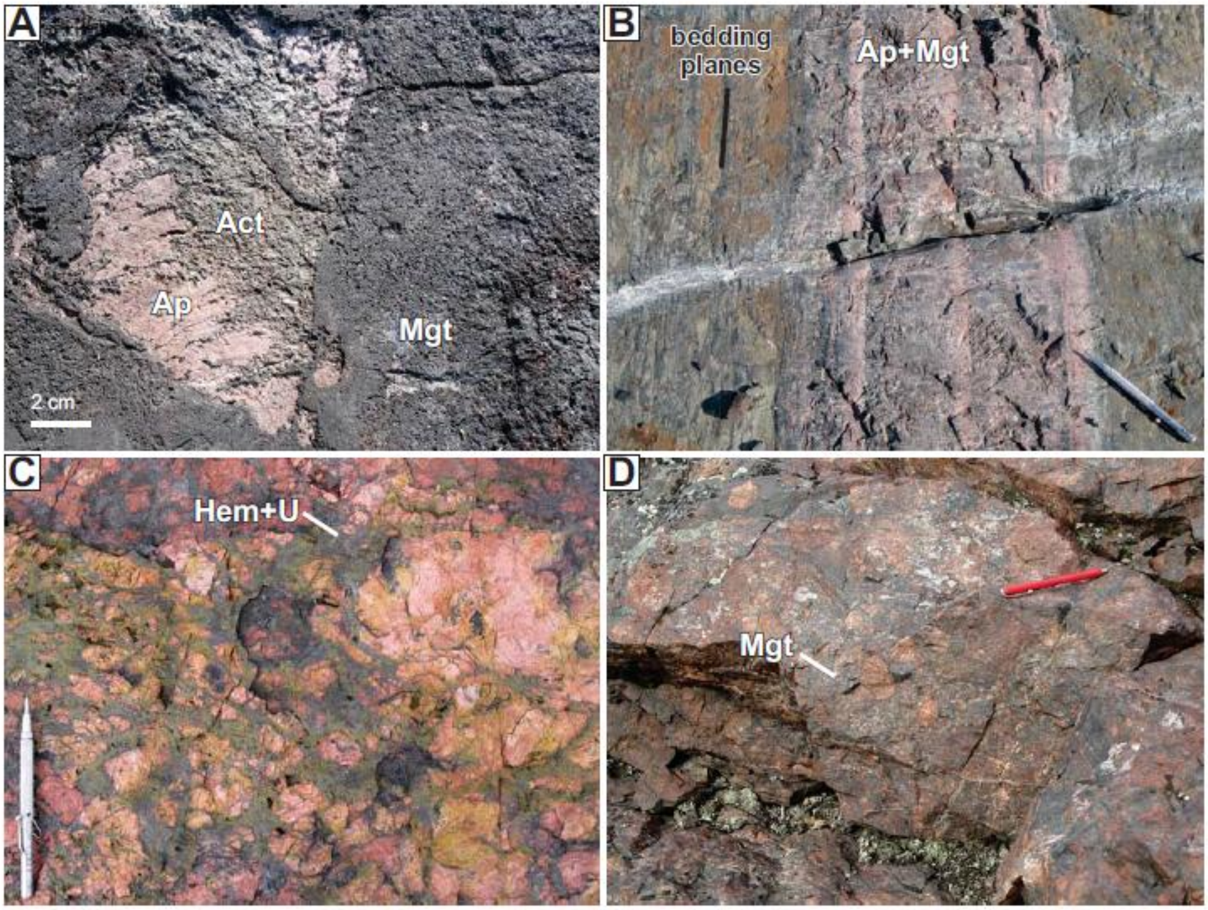

Figure 2

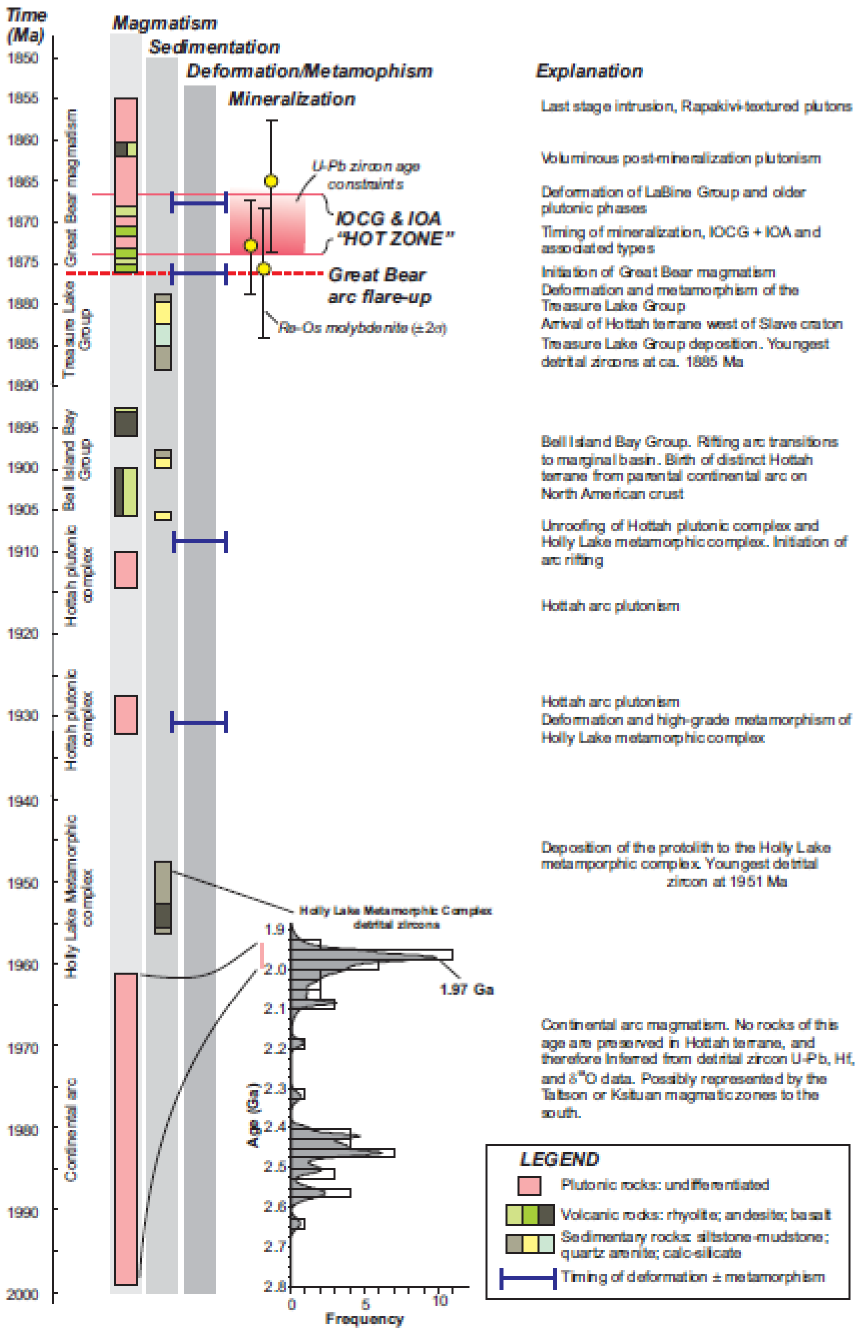

Time (Ma)
Magmatism
Sedimentation
Deformation/Metamophism
Mineralization
Explanation
Great Bear magmatism
Treasure Lake Group
Bell Island Bay Group
Hottah plutonic complex
Holly Lake Metamorphic complex
Continental arc
U-Pb zircon age constraints
IOCG & IOA "HOT ZONE"
Great Bear arc flare-up
Re-Os molybdenite (±2σ)
Last stage intrusion, Rapakivi-textured plutons
Voluminous post-mineralization plutonism
Deformation of LaBine Group and older plutonic phases
Timing of mineralization, IOCG + IOA and associated types
Initiation of Great Bear magmatism
Deformation and metamorphism of the Treasure Lake Group
Arrival of Hottah terrane west of Slave craton
Treasure Lake Group deposition. Youngest detrital zircons at ca. 1885 Ma
Bell Island Bay Group. Rifting arc transitions to marginal basin. Birth of distinct Hottah terrane from parental continental arc on North American crust
Unroofing of Hottah plutonic complex and Holly Lake metamorphic complex. Initiation of arc rifting
Hottah arc plutonism
Hottah arc plutonism
Deformation and high-grade metamorphism of Holly Lake metamorphic complex
Deposition of the protolith to the Holly Lake metamporphic complex. Youngest detrital zircon at 1951 Ma
Holly Lake Metamorphic Complex detrital zircons
1.97 Ga
Age (Ga)
Frequency
Continental arc magmatism. No rocks of this age are preserved in Hottah terrane, and therefore inferred from detrital zircon U-Pb, Hf, and δ18O data. Possibly represented by the Taltson or Ksituan magmatic zones to the south.
LEGEND
Plutonic rocks: undifferentiated
Volcanic rocks: rhyolite; andesite; basalt
Sedimentary rocks: siltstone-mudstone; quartz arenite; calc-silicate
Timing of deformation ± metamorphism

Figure 3

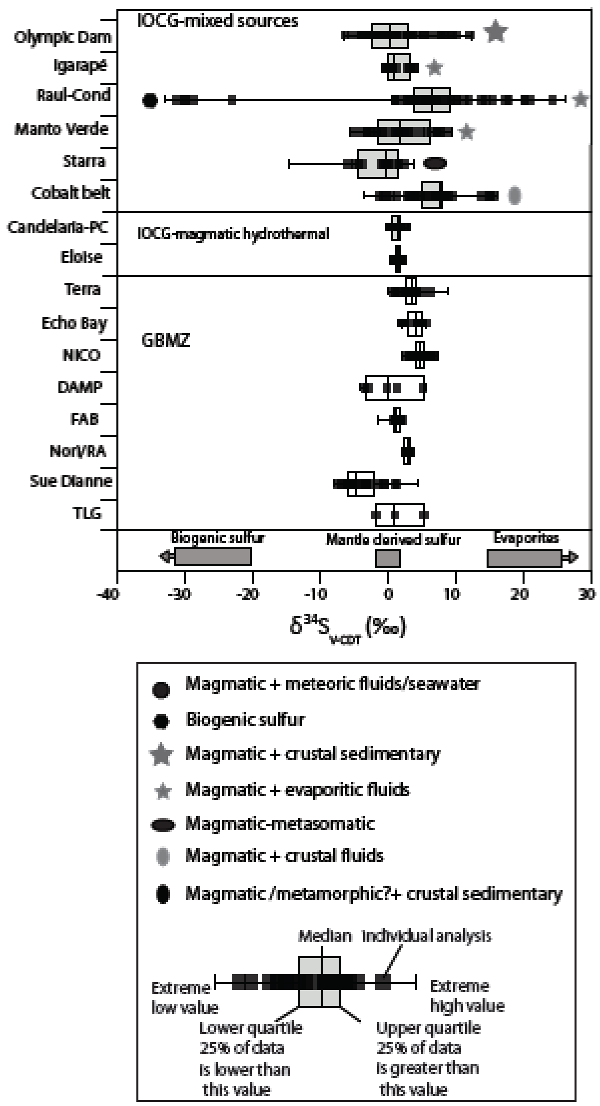

IOCG-mixed sources
Olympic Dam
Igarapé
Raul-Cond
Manto Verde
Starra
Cobalt belt
Candelaria-PC
Eloise
IOCG-magmatic hydrothermal
Terra
Echo Bay
GBMZ
NICO
DAMP
FAB
Nori/RA
Sue Dianne
TLG
Biogenic sulfur
Mantle derived sulfur
Evaporites
-40
-30
-20
-10
0
10
20
30
δ34S V-CDT (‰)
Magmatic + meteoric fluids/seawater
Biogenic sulfur
Magmatic + crustal sedimentary
Magmatic + evaporitic fluids
Magmatic-metasomatic
Magmatic + crustal fluids
Magmatic /metamorphic?+ crustal sedimentary
Median
Individual analysis
Extreme low value
Extreme high value
Lower quartile 25% of data is lower than this value
Upper quartile 25% of data is greater than this value

Figure 4

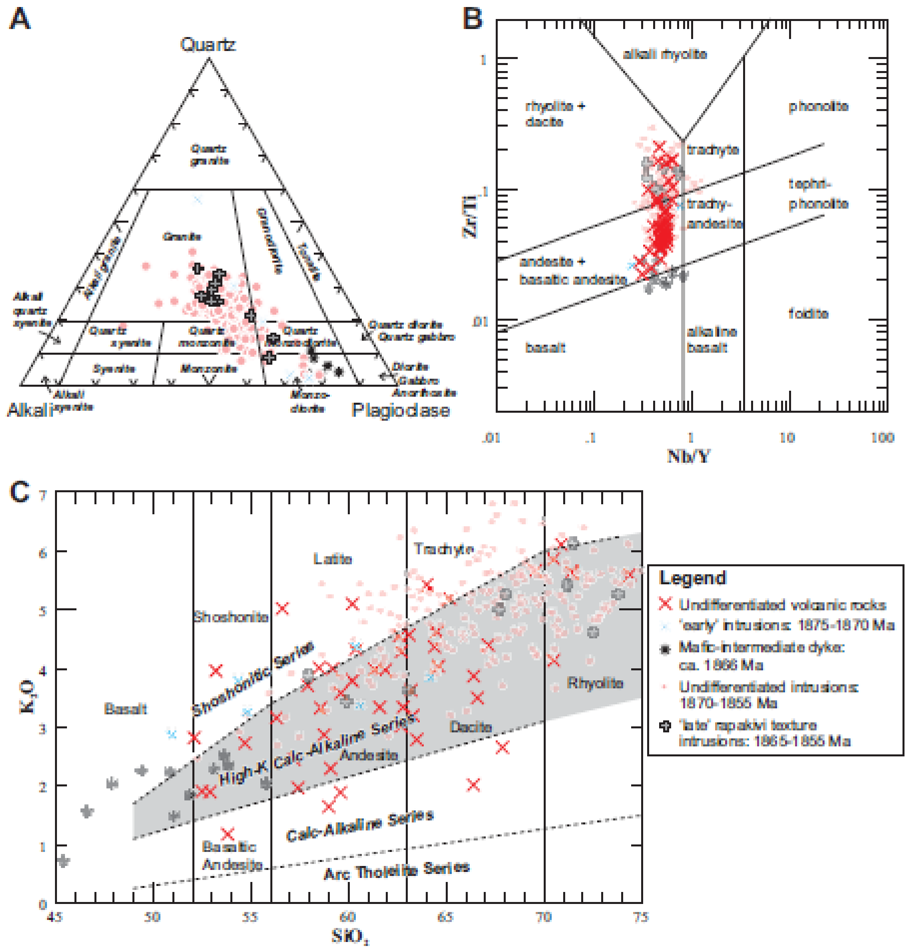
A
Quartz
Quartz granite
Granite
Alkali granite
Granodiorite
Tonalite
Alkali quartz syenite
Quartz syenite
Quartz monzonite
Quartz monzodiorite
Quartz diorite Quartz gabbro
Syenite
Monzonite
Diorite Gabbro Anorthosite
Alkali syenite
Monzo-diorite
Alkali
Plagioclase
B
alkali rhyolite
rhyolite + dacite
phonolite
trachyte
tephri-phonolite
trachy-andesite
andesite + basaltic andesite
foidite
basalt
alkaline basalt
Zr/Ti
Nb/Y
C
Latite
Trachyte
Shoshonite
Shoshonitic Series
Basalt
High-K Calc-Alkaline Series
Andesite
Dacite
Rhyolite
Calc-Alkaline Series
Basaltic Andesite
Arc Tholeiite Series
K_2O
SiO_2
Legend
Undifferentiated volcanic rocks
'early' intrusions: 1875-1870 Ma
Mafic-intermediate dyke: ca. 1866 Ma
Undifferentiated intrusions: 1870-1855 Ma
'late' rapakivi texture intrusions: 1865-1855 Ma

Figure 5

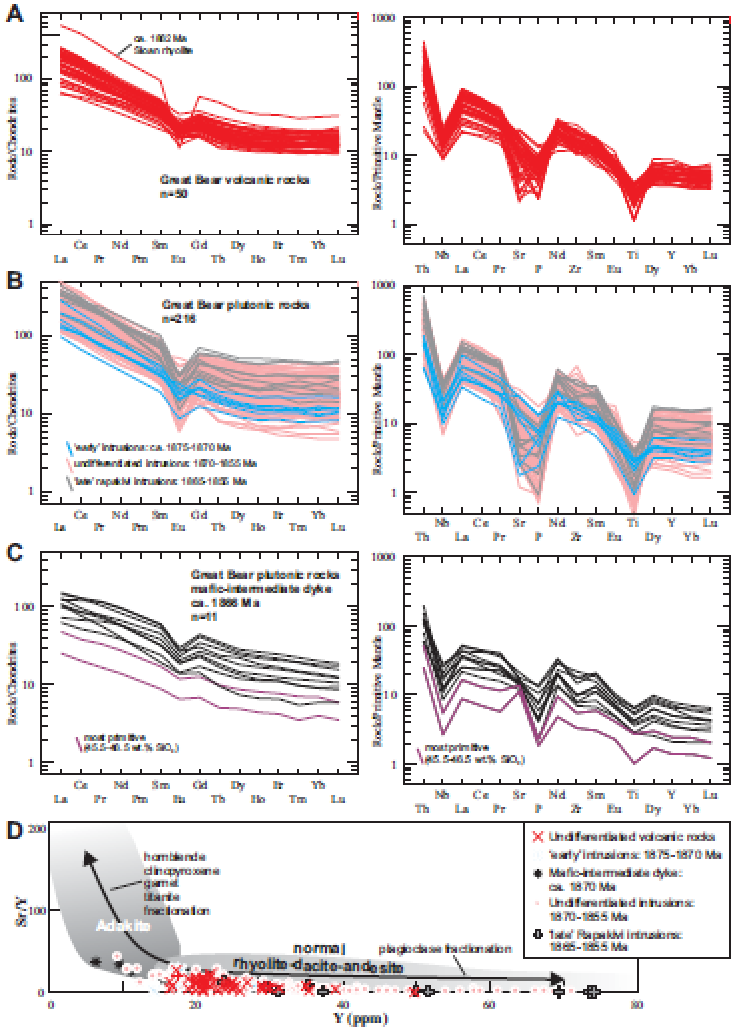
A
Great Bear volcanic rocks
n=50
B
Great Bear plutonic rocks
n=216
C
Great Bear plutonic rocks
mafic-intermediate dyke
D
Adakite
normal
rhyolite-dacite-andesite
plagioclase fractionation
Y (ppm)
Undifferentiated volcanic rocks

Figure 6

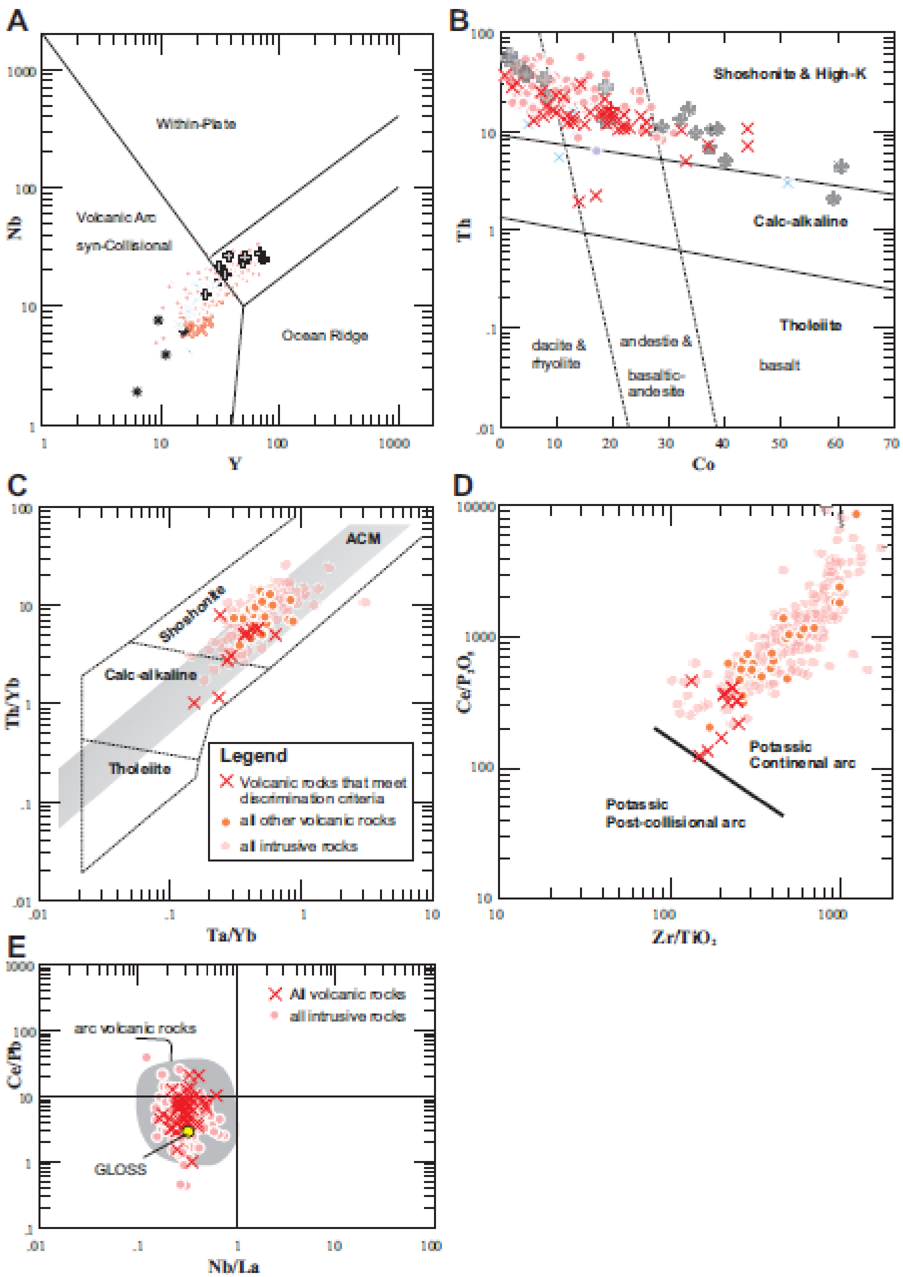
A
Within-Plate
Volcanic Arc
syn-Collisional
Ocean Ridge
Nb
Y
B
Shoshonite & High-K
Calc-alkaline
Tholeiite
dacite & rhyolite
andestie &
basaltic-andesite
basalt
Th
Co
C
ACM
Shoshonite
Calc-alkaline
Tholeiite
Legend
Volcanic rocks that meet discrimination criteria
all other volcanic rocks
all intrusive rocks
Th/Yb
Ta/Yb
D
Potassic Continenal arc
Potassic Post-collisional arc
Ce/P2O5
Zr/TiO2
E
All volcanic rocks
all intrusive rocks
arc volcanic rocks
GLOSS
Ce/Pb
Nb/La

Figure 7

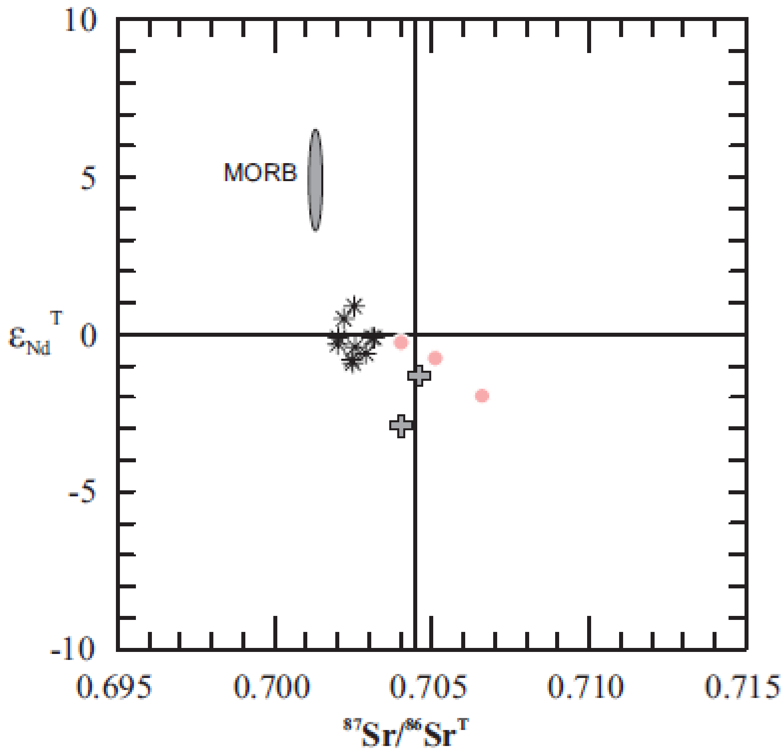

10
5
0
-5
-10
MORB
ε_{Nd}^{T}
0.695
0.700
0.705
0.710
0.715
$^{87}Sr/^{86}Sr^{T}$

Figure 8

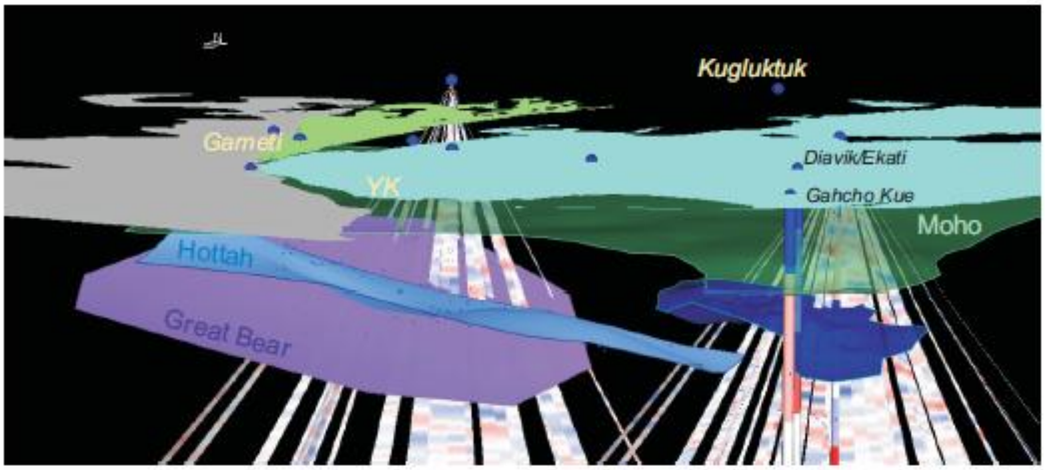
Kugluktuk
Gameti
YK
Diavik/Ekati
Gahcho Kue
Moho
Hottah
Great Bear

Figure 9

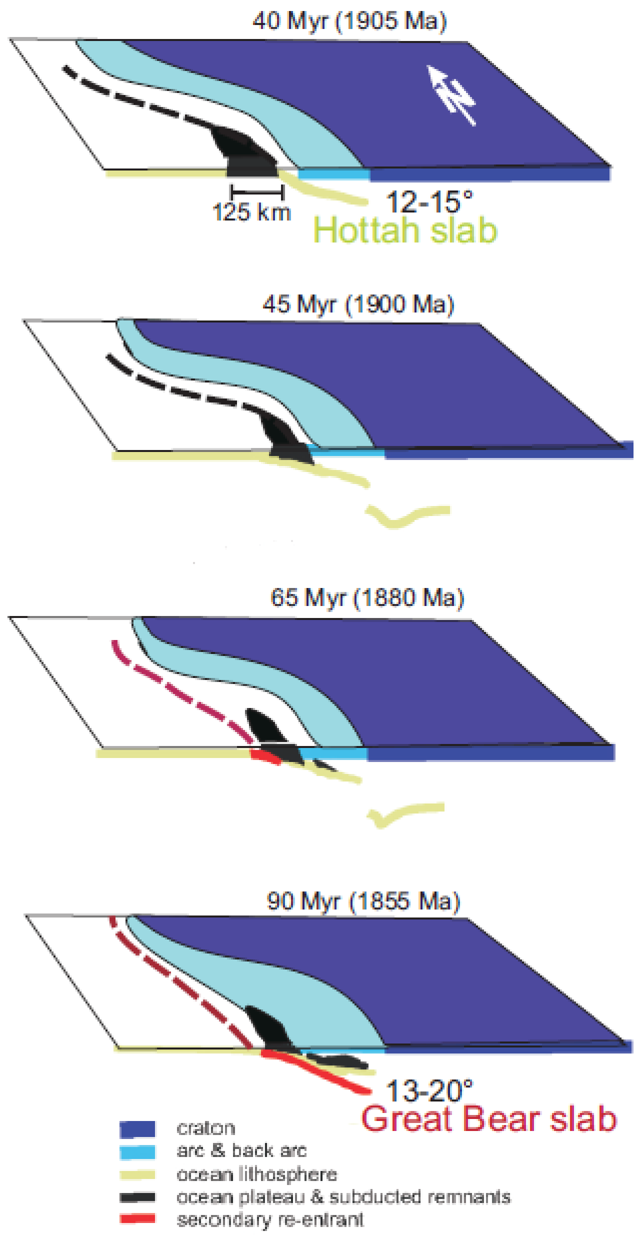
40 Myr (1905 Ma)
N
125 km
12-15°
Hottah slab
45 Myr (1900 Ma)
65 Myr (1880 Ma)
90 Myr (1855 Ma)
13-20°
Great Bear slab
craton
arc & back arc
ocean lithosphere
ocean plateau & subducted remnants
secondary re-entrant

Figure 10

Graphical abstract

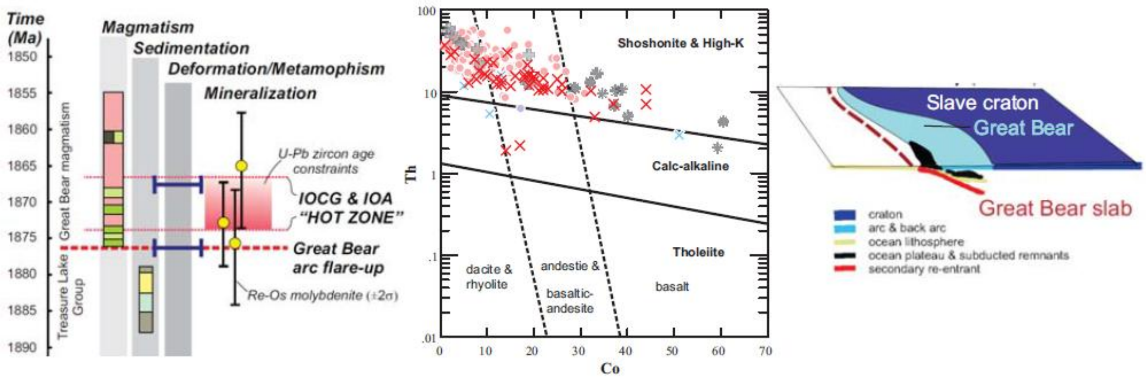

Great Bear IOCG paper highlights

Ootes et al. submission to OGR

- Great Bear magmatic zone is a Paleoproterozoic continental magmatic arc that hosts spatially and temporally related IOCG and IOA mineralization
- Mineralization occurred in a tight-time window between 1873 and 1866 Ma.
- New geochemistry demonstrates that magmatism is dominantly shoshonitic in nature
- 3D geophysical modelling demonstrates two arrested, east-dipping slabs
- Magmatism and IOCG-IOA mineralization related to Andean-like convergent margin

Table 1: Summary of prospects in the GBMZ (Modified after Montrieul et al., in review)

	Prospect/DepositProspect/Deposit	*Principal Metals*	*Deposit Types*	*Host rocks*
Port-Radium-Echo Bay District	**Port Radium**	U	Epithermal	1.87 Ga LaBine volcaniclastic and sedimentary (siliciclastic)
		Cu,Ag,Co,Bi,Zn,Pb	Epithermal	
		Fe,V	IOA	
	Sloan	Cu	Epithermal, IOCG	
	Mariner	Cu	Epithermal, IOCG	
	Echo Bay	Cu, Ag, Co, Bi, Zn, Pb, Au	IOA, IOCG	
	Camelback	Cu,Zn,Pb,Ag,U,V,Co,Au	Epithermal, IOCG	1.87 Ga LaBine andesite
	K2	Cu,Ag,Co,Au,	IOA, IOCG	
	Mag Hill	Fe,V	IOA	
	Skinny Lake	Ag,Cu,Zn,Pb	IOCG (Hem)	
	Contact Lake End	Fe	IOA	
	Hook Island	Au,Ag,U,Cu	IOCG (Mag, Hem)	
	Mile Lake	Cu,Zn,Pb,Ag, Mo, W	IOCG - Skarn	1.87 Ga LaBine volcaniclastic
Camsell River District	**Terra,Norrex, Silver Bear**	Cu,Ag,U,Co,Bi,Zn,Pb,Au,Fe-V	Epithermal, IOA, IOCG	1.87 Ga LaBine Gp volcano-sedimentary
	Grouard W Clutt, Bar	Au,Ag,Cu,Pb	IOCG	

			(Mag, Hem)	
	Grouard N to NE	?	IOCG	
	Grouard S (Ness, Hillside)	Zn,Pb,Ag	Skarn	
Central	Damp	Cu,U	IOCG (Hem)	1.87 Ga rhyodacitic ignimbrite
	Devil	Au,Ag,Co,Cu,As, Fe,Pb		
Wopmay fault	Jackpot, McPhoo	U,Cu,Fe,REE,Th,Co,Bi,Au,Mo	IOA, IOCG (Mag)	1.87 Ga porphyritic intrusions and Dumas volcano-sedimentary rocks
	Ham	U,Fe,Cu,REE	IOA, IOCG	
	JLD	U,Cu,Fe,REE	IOA, IOCG	
De-Vries	De Vries, NORI	U,Mo,Fe,Cu	Intrusion	1.88 Ga Treasure Lake sedimentary rocks
Fab	Fab	U,Cu,Fe,V	IOA, IOCG (Mag)	1.87 Ga porphyritic intrusions
Mazenod	**Sue Dianne**	Cu,Ag,Au,U	IOCG (Mag, Hem)	1.87 Ga Faber dacite to andesite
	Nod	Cu-Fe	IOA to IOCG (Mag) - skarn	
	Brooke	Cu,Ag,Fe,Bi,Mo, REE	IOCG (Mag, Hem)	
Eastern Treasure Lake	Cole	U,Fe	Albitite	1.88 Ga Treasure Lake sedimentary rocks & 1.87 Ga intrusions
	Ron	Fe,REE	IOA	
	Hump	Fe,V,REE	IOA	
	Peanut Lake	Fe	IOA	
	Esther	U,Ta,Ag,Cu	?	
	Carbonate Mountain	Cu, Pb, Zn, Ag	Skarn	
Duke	Duke	Co,Bi,Au,Cu,Fe,REE	IOCG (Mag, Hem)	1.88 Ga Treasure Lake sedimentary rocks
	LP's	W,Fe	IOCG (Mag)	
	LJLVS	Co,Ni,U,Cu,Fe	IOCG	

			(Mag)	
	Rayrock	U,Cu	Epithermal	1.87 Ga Faber dacite to andesite
Lou	Southern Breccia	U,Cu,Mo,Th,Au,Bi	Albitite	1.88 Ga Treasure Lake sedimentary rocks & 1.87 Ga intrusions
	NICO	Co, Au, Bi, Cu, W, Fe	IOCG (Mag)	

IOCG - iron oxide copper-gold type; IOA - iron oxide (magnetite) apatite ± actinolite type; Epithermal - quartz or quartz-carbanate vein-hosted; skarn - skarn type; Intrusion - intrusion-related; Albitite - albitite-hosted uranium

Mag - magnetite; Hem – hematite